

Fig. 6. Endocrine Disruption of RXR:PPAR γ Signaling and Ectopic Induction of Adipocytes in *X. laevis* by TBT

A, Expression levels of *Xenopus* aromatase (XCYP19) were determined in tadpoles (stage 56) by quantitative real-time PCR after 24-h exposure to vehicle only (DMSO) or the indicated ligands. Expression was normalized to *Xenopus* EF1 α and expressed as average fold change in expression \pm SEM (n = 9) relative to vehicle controls. B, *X. laevis* tadpoles were dosed weekly under static renewal conditions with indicated ligands from stage 48 (before gonadogenesis) until stage 64 (metamorphic climax). Metamorphs (stage 66) were scored for ectopic adipocyte patches on gonads and urogenital ducts. Data are shown as the percentage of metamorphs exhibiting ectopic adipocyte patches posterior to the fat bodies; mean \pm SD from triplicate tanks. C–E, Dissecting microscope photographs of kidneys (k), testis (t), and fat bodies (fb) from DMSO control, 10 nM TBT, and 1 μ M troglitazone-treated male metamorphs. Multiple ectopic adipocyte patches (red arrows) are present posterior to the fat bodies along the anterior-posterior axis of gonads in TBT (D)- and troglitazone (E)-treated animals but not controls (C). Histological sections of kidneys and gonads from the same control (F) and 10 nM TBT (G)-treated males at the level indicated by the white line in C and D. Gonadal and connective tissue was either completely replaced by, or interspersed with, adipocytes (red arrows) in TBT-treated animals. Sections were developed with Mallory's trichrome stain. Scale bars, 100 μ m.

maceutical therapies for type 2 diabetes that can also promote obesity by increasing fat storage. Likewise, RXR ligands also act as insulin-sensitizing agonists in rodents (61), underscoring the permissive nature of the PPAR γ :RXR heterodimer and the potential effects on diabetes and obesity of both PPAR γ and RXR agonists.

Our data are consistent with recent studies that organotins can mediate some of their endocrine dis-

ruption effects by transcriptional regulation through nuclear receptors, in particular RXR:PPAR γ signaling (17–19, 24). Consequently, TBT exposure can promote adipocyte differentiation in the same manner as other RXR or PPAR γ ligands *in vitro* using the standard murine 3T3-L1 cell model and *in vivo* through increased adiposity after intrauterine organotin exposure in newborn mice. It is currently unknown whether the increased adiposity *in vivo* results from an increase

in adipocyte precursor cell number, enhanced adipocyte differentiation from the same number of precursors, an increase in adipocyte size without an increase in number, or some combination of these.

The prevailing epidemiological data ascribe high-density caloric and/or fatty diets coupled with decreased physical activity as the root causes for the rise in obesity rates in the general population (62). The contribution of genetic components is less clear. Although genetic variation contributes to an individual's propensity to develop obesity, the rapid worldwide increase in obesity suggests that interaction with the modern environment exposes inherent genetic differences. The Barker hypothesis postulates that *in utero* fetal nutritional status is a potential risk factor for metabolic syndrome diseases (63–67). In this view, developmental metabolic programming of a thrifty phenotype limits the range in adaptive responses to the environment, e.g. diet and exercise, in later life (68). Experimental evidence from animal models lends support to this hypothesis (69). Plausible mechanisms include imprinting of obesity-sensitive hormonal pathways or changes in cell type and number, e.g. adipocytes, established during development.

Others, however, argue that the environment plays another role in obesity. Because the increase in obesity rates parallels the rapid growth in the use of industrial chemicals over the past 40 yr, it is plausible and provocative to associate *in utero* or chronic lifetime exposure to chemical triggers present in the modern environment with this epidemic. Hence, an "obesogen" model predicts the existence of xenobiotic chemicals that inappropriately regulate lipid metabolism and adipogenesis to promote obesity. Several recent studies serve as proof-of-principle for such a hypothesis. Environmental estrogens such as bisphenol A and nonylphenol, for instance, can promote adipocyte differentiation or proliferation in murine cell lines (70, 71). Furthermore, epidemiological studies link maternal smoking during pregnancy to an elevated risk of childhood obesity (72–76).

Seen in this context, we propose that organotins such as TBT and its congeners are chemical stressors or obesogens that activate RXR:PPAR γ signaling to promote long-term changes in adipocyte number and/or lipid homeostasis after developmental or chronic lifetime exposure.

MATERIALS AND METHODS

Plasmids and Transfections

pCMX-GAL4 and pCMX-VP16 plasmid fusion constructs to nuclear receptor LBDs and coactivators [GAL4-hRAR α , hRXR α , -xRXR α/γ , -hPPAR γ , -mPPAR α , -human steroid and xenobiotic receptor (SXR), -NURR1, -VDR, -LXR, -hACTR, -hPPAR-binding protein (PBP), -human steroid receptor coactivator-1 (SRC-1), human transcriptional intermediary factor 2 (TIF2)] have been previously described (77–82). Transfections were performed in Cos7 cells (transformed green

monkey kidney fibroblast cell line) essentially as described elsewhere (83) using MH200-x4-TK-Luc as reporter and normalized to pCMX- β -galactosidase controls. Briefly, Cos7 cells were seeded at 5000 cells per well in 96-well tissue culture plates in 10% fetal bovine serum/DMEM and transfected for 8 h with 11 μ g/plate of DNA/calcium phosphate precipitate mix (MH200x4-TK-Luc-CMX- β -galactosidase-nuclear receptor/coactivator effector(s) at a ratio of 5:5:1). Cells were washed free of precipitate with PBS and media were replaced with serum-free insulin, transferrin, lipid, bovine serum albumin supplemented (ITLB)/DMEM (84) plus ligands for an additional 24 h before assays for luciferase and β -galactosidase activity. All transfection data points were performed in triplicate, and all experiments were repeated at least three times.

Quantitative Real-Time PCR Analyses

Total cellular RNA from C57BL/6 mouse and *X. laevis* tissues was isolated with Trizol reagent and reversed transcribed with oligo dT and Superscript II (Invitrogen, San Diego, CA) according to the manufacturer's instructions. Triplicate cDNA samples (50 ng/reaction) were analyzed by quantitative real-time PCR on a DNA Engine Opticon thermal cycler [MJ Research (Watertown, MA)/Bio-Rad Laboratories (Hercules, CA)] using SYBR Green chemistry (PerkinElmer Life Sciences, Wellesley, MA). Fold changes in expression levels were calculated after normalization to histone Hist2h4 using the $\Delta\Delta$ cycle threshold method (85). Gene-specific primers were as follows. Hist2h4 forward (F): 5'-CCCGTGGTGTGC-TGAAGGTGTT-3'; reverse (R), 5'-GAATTGAAGCGGCGCG-GTCTA-3'; RXR α F: 5'-CGGCTGCTCAGGGTACTTGTGTTT-3'; R, 5'-CGGCTGCTCAGGGTACTTGTGTTT-3'; PPAR γ F: 5'-TGGGTGAAACTCTGGGAGATTC-3'; R, 5'-AATTTCTTG-TGAAGTGCTCATAGGC-3'; C/EBP α F: 5'-CCAAGAAGTCG-TGGACAAGA-3'; R, 5'-CGGTCAATGTCACTGGTCAACT-3'; C/EBP β F: 5'-GCCCGCCGCTTTAGACC-3'; R, 5'-CG-CTCGTCTCGCCAATG-3'; C/EBP δ F: 5'-AACCCGCGGC-CTTCTACGAG-3'; R, 5'-ACGGCGCCATGGAGTCAAT-3'; aP2 F: 5'-GAATTCGATGAAATCACCAGCA-3'; R, 5'-CTCTTT-ATTGTGGTTCGACTTTCCA-3'; FATP F: 5'-AGCCGCTTCTG-GGATGACTGTGT-3'; R, 5'-ACCGAAGCGCTGCGTGAA-CTC-3'; ACS F: 5'-CCCAGCCAGTCCCCACCAG-3'; R, 5'-CACACCACTCAGGCTCACACTCGT-3'; FASN F: 5'-TCGG-GTGTGGTGGGTTTGGTGAAT-3'; R, 5'-ACTTGGGGCGGT-GAGATGTGTTGC-3'; ACAC F: 5'-G GATGGCAGCTCTGGA-GGTGTATG-3'; R, 5'-TGTCTTAAGCTGGCGGTGTGTA; Pck1 F: 5'-CTGGCAGCATGGGGTGTGTTGTAGG-3'; R, 5'-TGCCGAAGTTGTAGCCGAAGAAGG-3'; Srebf1 F: 5'-GCC-CCTGCCACCTCAAACCT-3'; R, 5'-ACTGGCACGGGCAT-CCCTCCTC-3'; *Xenopus* EF1 α F: 5'-GATCCCAGGAAAGC-CAATGTGC 3'; R, 5'-CCGATCCTGCTGCCTTCTTCT-3'; *Xenopus* CYP19 (aromatase) F: 5'-GTCTGGATTAATGGCGAG-GAAACA-3'; R, 5'-CTGATGAAGTATGGCCGAATGACC-3'.

Ligand Binding

Histidine-tagged RXR α LBD (H_6 -RXR α LBDs) was expressed and purified from pET15b(+) vector in BL21(DE3) pLysS bacteria cultures after induction with 1 mM isopropyl- β -D-thiogalactopyranoside for 3 h at 37 C (86). Purified H_6 -PPAR γ was purchased from Invitrogen. Proteins were bound to 96-well Nickel Chelate Flashplates (PerkinElmer Life Sciences) at 100 μ g/ml overnight at 4 C and washed five times with 200 μ l/well Flashplate Assay Buffer (20 mM HEPES, pH 7.9; 100 mM KCl, 0.1% cholesterylpropylidimethylammonio-2-hydroxy-1-propanesulfonate, 0.1 mM dithiothreitol). Competition assays typically used 1–5 nM [3 H]-9-*cis*-RA (PerkinElmer Life Sciences) or 10–50 nM [3 H]rosiglitazone (American Radiochemicals, Inc., St. Louis, MO) plus cold competitor ligands in Flashplate Assay Buffer at concentrations indicated in the figures. Plates were incubated at room temperature, pro-

tected from light, and read after 4 h on a Packard Topcount scintillation counter (Packard Instruments, Meriden, CT). Specific bound counts/min were determined by subtraction of counts/min from uncoated wells at each ligand concentration. Data were analyzed with GraphPad Prism 4.0 (GraphPad Software, Inc., San Diego, CA) using a one-site competition binding equation to determine K_d values for competitor ligands; K_d values of 1.4 and 41 nM for 9-*cis*-RA and rosiglitazone for their respective receptors were used in the calculations (87, 88).

3T3-L1 Cell Assays

3T3-L1 (American Type Culture Collection, Manassas, VA) cells were maintained as subconfluent cultures by passage every 3 d from cultures seeded at 5000 cells/cm² in 8% calf serum/DMEM. For differentiation assays, cells were seeded at 15×10^3 cells per well into 24-well tissue culture plates in 8% fetal bovine serum/DMEM, after which cultures were grown for 2 d and then treated with the indicated RXR, RAR, and PPAR ligands either with or without MDIT (100 μ M 3-isobutyl-1-methylxanthine, 100 nM dexamethasone, 0.1 ng/ml insulin, and 2 nM T₃ thyroid hormone) induction cocktail. Media and ligand treatments were renewed every 2 d. After 1 wk, cells were scored for adipocyte differentiation by Oil Red O staining for lipid droplet accumulation. Cultures were washed with PBS, fixed with 10% formaldehyde for 15 min, washed with distilled water, and stained with filtered Oil Red O solution (4 g/liter, 60% isopropanol) for 15 min. Excess stain was removed by washing three times with distilled water. Three random fields from each well were photographed under phase contrast and analyzed in ImageJ. Images were converted into high-contrast black and white images to visualize lipid droplets and scored as the percentage area per field. Data are shown as the mean \pm SEM from three wells per treatment. The method was validated by extraction of Oil Red O from stained cells into 100% isopropanol and quantitated by absorbance at 540 nm on a spectrophotometer.

In Vivo Animal Exposure Experiments

C57BL/6J mice were housed under a 12-h light, 12-h dark cycle. Pregnant mice were dosed by ip injection with TBT [0.05 or 0.5 mg/kg body weight (b.w.)] or vehicle (sesame oil) from embryonic d 12 (E12) every 24 h until the day before delivery. Neonates were killed at the day of delivery and analyzed. The samples were embedded in optimal cutting temperature embedding compound and sectioned (12 mm) using a cryostat. Sections were fixed on slides with 4% paraformaldehyde for 10 min and rinsed in PBS. The slides were then sequentially washed with distilled water and 60% of isopropanol and stained with Oil Red O (4 g/liter, 60% isopropanol). After washing with 60% isopropanol and distilled water, the slides were counterstained with hematoxylin. Sections were evaluated and photographed using a Zeiss microscope (Carl Zeiss, Thornwood, NY).

For long-term growth studies, pups were cross-fostered to unexposed C57BL/6 dams after birth, and litter sizes were kept constant at eight pups per dam (control, two male + two female; TBT treated, two male + two female). Animals were weaned at 3 wk of age and maintained on standard rodent chow. Total body weight was followed until 10 wk of age. Males were then killed, and epididymal fat pads were dissected and weighed.

X. laevis tadpoles were sorted at stage 48 (89) and maintained in 1-liter glass tanks in 20% Holtfreter's buffered salt solution (90) at a density of 10 tadpoles per tank on a diet of ground Tetraamin Fish Flakes and spirulina. Compounds prepared in dimethylsulfoxide (DMSO) as 10⁵-fold stock solutions were tested on triplicate tanks and dosed by static renewal after weekly water changes. Metamorphs at stage 64

were transferred to individual containers and fed frozen brine shrimp for 2 wk until stage 66. Froglets were euthanized with 250 mg/liter MS222 in 20% Holtfreter's solution and then scored for gonadal abnormalities and interrenal/gonadal adipocyte formation under a dissecting microscope. Kidneys with attached gonads and livers were fixed in 10% formalin-PBS, embedded in paraffin, and sectioned at 15 μ m thickness. Sections were developed with Mallory's trichrome stain.

All animal experiments were approved and performed in accordance with Institutional Animal Care and Use Committee protocols.

Acknowledgments

We thank Drs. I. Blitz, K. Cho, C. Zhou, and T. Osborne for critical reading and comments on the manuscript, Dr. C. Li (Expression Technologies) for the H₆-RXR α LBD construct, and Dr. R. Chandraratna (Allergan Pharmaceuticals, Irvine, CA) for AGN203 and LG268.

Received September 8, 2005. Accepted March 30, 2006.

Address all correspondence and requests for reprints to: Bruce Blumberg, Department of Developmental and Cell Biology, University of California Irvine, 2113 McGaugh Hall, Irvine, California 92697-2300. E-mail: blumberg@uci.edu.

This work was supported by grants from the U.S. Environmental Protection Agency (STAR R830686) and National Institutes of Health (GM-60572) (to B.B.); from the Ministries of Education, Culture, Sports, Science and Technology, Environment and Health Labor and Welfare, Japan (to T.I.); and from the University of California Toxic Substance Research and Training Program (UC-37579) (to F.G.).

F.G., H.W., Z.Z., L.M., K.A., R.C., D.M.G., J.K., T.I. have nothing to declare. B.B. is a named inventor on U.S. patents US 5,861,274, US 6,200,802, and US 6,815,168.

REFERENCES

1. Appel KE 2004 Organotin compounds: toxicokinetic aspects. *Drug Metab Rev* 36:763–786
2. Golub M, Doherty J 2004 Triphenyltin as a potential human endocrine disruptor. *J Toxicol Environ Health B Crit Rev* 7:281–295
3. Blaber SJM 1970 The occurrence of a penis-like outgrowth behind the right tentacle in spent females of *Nucella lapillus*. *Proc Malacolog Soc London* 39:231–233
4. Gibbs P, Bryan G 1986 Reproductive failure in populations of the dogwhelk, *Nucella lapillus*, caused by imposex induced by tributyltin from antifouling paints. *J Mar Biol Assoc UK* 66:767–777
5. Matthiessen P, Gibbs P 1998 Critical appraisal of the evidence for tributyltin-mediated endocrine disruption in mollusks. *Environ Toxicol Chem* 17:37–43
6. Shimasaki Y, Kitano T, Oshima Y, Inoue S, Imada N, Honjo T 2003 Tributyltin causes masculinization in fish. *Environ Toxicol Chem* 22:141–144
7. McAllister BG, Kime DE 2003 Early life exposure to environmental levels of the aromatase inhibitor tributyltin causes masculinisation and irreversible sperm damage in zebrafish (*Danio rerio*). *Aquat Toxicol* 65:309–316
8. Omura M, Ogata R, Kubo K, Shimasaki Y, Aou S, Oshima Y, Tanaka A, Hirata M, Makita Y, Inoue N 2001 Two-generation reproductive toxicity study of tributyltin chloride in male rats. *Toxicol Sci* 64:224–232
9. Ogata R, Omura M, Shimasaki Y, Kubo K, Oshima Y, Aou S, Inoue N 2001 Two-generation reproductive toxicity

- study of tributyltin chloride in female rats. *J Toxicol Environ Health A* 63:127–144
10. Boyer IJ 1989 Toxicity of dibutyltin, tributyltin and other organotin compounds to humans and to experimental animals. *Toxicology* 55:253–298
 11. Heidrich DD, Steckelbroeck S, Klingmuller D 2001 Inhibition of human cytochrome P450 aromatase activity by butyltins. *Steroids* 66:763–769
 12. Cooke GM 2002 Effect of organotins on human aromatase activity in vitro. *Toxicol Lett* 126:121–130
 13. Powers MF, Beavis AD 1991 Triorganotins inhibit the mitochondrial inner membrane anion channel. *J Biol Chem* 266:17250–17256
 14. Gennari A, Viviani B, Galli CL, Marinovich M, Pieters R, Corsini E 2000 Organotins induce apoptosis by disturbance of $[Ca^{2+}]_i$ and mitochondrial activity, causing oxidative stress and activation of caspases in rat thymocytes. *Toxicol Appl Pharmacol* 169:185–190
 15. Philbert MA, Billingsley ML, Reuhl KR 2000 Mechanisms of injury in the central nervous system. *Toxicol Pathol* 28:43–53
 16. Mu YM, Yanase T, Nishi Y, Waseda N, Oda T, Tanaka A, Takayanagi R, Nawata H 2000 Insulin sensitizer, troglitazone, directly inhibits aromatase activity in human ovarian granulosa cells. *Biochem Biophys Res Commun* 271:710–713
 17. Mu YM, Yanase T, Nishi Y, Takayanagi R, Goto K, Nawata H 2001 Combined treatment with specific ligands for PPAR γ :RXR nuclear receptor system markedly inhibits the expression of cytochrome P450arom in human granulosa cancer cells. *Mol Cell Endocrinol* 181:239–248
 18. Saitoh M, Yanase T, Morinaga H, Tanabe M, Mu YM, Nishi Y, Nomura M, Okabe T, Goto K, Takayanagi R, Nawata H 2001 Tributyltin or triphenyltin inhibits aromatase activity in the human granulosa-like tumor cell line KGN. *Biochem Biophys Res Commun* 289:198–204
 19. Nishikawa J, Mamiya S, Kanayama T, Nishikawa T, Shiraishi F, Horiguchi T 2004 Involvement of the retinoid X receptor in the development of imposex caused by organotins in gastropods. *Environ Sci Technol* 38:6271–6276
 20. Baillie-Hamilton PF 2002 Chemical toxins: a hypothesis to explain the global obesity epidemic. *J Altern Complement Med* 8:185–192
 21. Heindel JJ 2003 Endocrine disruptors and the obesity epidemic. *Toxicol Sci* 76:247–249
 22. Jacobs MN, Lewis DF 2002 Steroid hormone receptors and dietary ligands: a selected review. *Proc Nutr Soc* 61:105–122
 23. Watanabe H, Iguchi T, Morohashi K 2002 [Endocrine disruptors and nuclear receptors]. *Nippon Rinsho* 60:397–403
 24. Kanayama T, Kobayashi N, Mamiya S, Nakanishi T, Nishikawa J 2005 Organotin compounds promote adipocyte differentiation as agonists of the peroxisome proliferator-activated receptor γ /retinoid X receptor pathway. *Mol Pharmacol* 67:766–774
 25. Wang Z, Benoit G, Liu J, Prasad S, Aarnisalo P, Liu X, Xu H, Walker NP, Perlmann T 2003 Structure and function of Nurr1 identifies a class of ligand-independent nuclear receptors. *Nature* 423:555–560
 26. Aarnisalo P, Kim CH, Lee JW, Perlmann T 2002 Defining requirements for heterodimerization between the retinoid X receptor and the orphan nuclear receptor Nurr1. *J Biol Chem* 277:35118–35123
 27. Boehm MF, Zhang L, Zhi L, McClurg MR, Berger E, Wagoner M, Mais DE, Suto CM, Davies JA, Heyman RA, Nadzant AM 1995 Design and synthesis of potent retinoid X receptor selective ligands that induce apoptosis in leukemia cells. *J Med Chem* 38:3146–3155
 28. Yu C, Chen L, Luo H, Chen J, Cheng F, Gui C, Zhang R, Shen J, Chen K, Jiang H, Shen X 2004 Binding analyses between human PPAR γ -LBD and ligands. *Eur J Biochem* 271:386–397
 29. Forman BM, Tontonoz P, Chen J, Brun RP, Spiegelman BM, Evans RM 1995 15-Deoxy- δ 12, 14-prostaglandin J2 is a ligand for the adipocyte determination factor PPAR γ . *Cell* 83:803–812
 30. Schoonjans K, Staels B, Auwerx J 1996 The peroxisome proliferator activated receptors (PPARs) and their effects on lipid metabolism and adipocyte differentiation. *Biochim Biophys Acta* 1302:93–109
 31. Kersten S 2002 Peroxisome proliferator activated receptors and obesity. *Eur J Pharmacol* 440:223–234
 32. Lane MD, Tang QQ, Jiang MS 1999 Role of the CCAAT enhancer binding proteins (C/EBPs) in adipocyte differentiation. *Biochem Biophys Res Commun* 266:677–683
 33. Tang QQ, Otto TC, Lane MD 2003 CCAAT/enhancer-binding protein β is required for mitotic clonal expansion during adipogenesis. *Proc Natl Acad Sci USA* 100:850–855
 34. Tang QQ, Lane MD 1999 Activation and centromeric localization of CCAAT/enhancer-binding proteins during the mitotic clonal expansion of adipocyte differentiation. *Genes Dev* 13:2231–2241
 35. Rubin CS, Hirsch A, Fung C, Rosen OM 1978 Development of hormone receptors and hormonal responsiveness in vitro. Insulin receptors and insulin sensitivity in the preadipocyte and adipocyte forms of 3T3-L1 cells. *J Biol Chem* 253:7570–7578
 36. Kletzien RF, Clarke SD, Ulrich RG 1992 Enhancement of adipocyte differentiation by an insulin-sensitizing agent. *Mol Pharmacol* 41:393–398
 37. Kletzien RF, Foellmi LA, Harris PK, Wyse BM, Clarke SD 1992 Adipocyte fatty acid-binding protein: regulation of gene expression in vivo and in vitro by an insulin-sensitizing agent. *Mol Pharmacol* 42:558–562
 38. Tafuri SR 1996 Troglitazone enhances differentiation, basal glucose uptake, and Glut1 protein levels in 3T3-L1 adipocytes. *Endocrinology* 137:4706–4712
 39. Xue JC, Schwarz EJ, Chawla A, Lazar MA 1996 Distinct stages in adipogenesis revealed by retinoid inhibition of differentiation after induction of PPAR γ . *Mol Cell Biol* 16:1567–1575
 40. Kawada T, Kamei Y, Sugimoto E 1996 The possibility of active form of vitamins A and D as suppressors on adipocyte development via ligand-dependent transcriptional regulators. *Int J Obes Relat Metab Disord* 20(Suppl 3):S52–S57
 41. Kawada T, Kamei Y, Fujita A, Hida Y, Takahashi N, Sugimoto E, Fushiki T 2000 Carotenoids and retinoids as suppressors on adipocyte differentiation via nuclear receptors. *Biofactors* 13:103–109
 42. Tontonoz P, Graves RA, Budavari AI, Erdjument-Bromage H, Lui M, Hu E, Tempst P, Spiegelman BM 1994 Adipocyte-specific transcription factor ARF6 is a heterodimeric complex of two nuclear hormone receptors, PPAR γ and RXR α . *Nucleic Acids Res* 22:5628–5634
 43. Martin G, Schoonjans K, Lefebvre AM, Staels B, Auwerx J 1997 Coordinate regulation of the expression of the fatty acid transport protein and acyl-CoA synthetase genes by PPAR α and PPAR γ activators. *J Biol Chem* 272:28210–28217
 44. Motojima K, Passilly P, Peters JM, Gonzalez FJ, Latruffe N 1998 Expression of putative fatty acid transporter genes are regulated by peroxisome proliferator-activated receptor α and γ activators in a tissue- and inducer-specific manner. *J Biol Chem* 273:16710–16714
 45. Frohnert BI, Hui TY, Bernlohr DA 1999 Identification of a functional peroxisome proliferator-responsive element in the murine fatty acid transport protein gene. *J Biol Chem* 274:3970–3977
 46. Martin G, Poirier H, Hennuyer N, Crombie D, Fruchart JC, Heyman RA, Besnard P, Auwerx J 2000 Induction of the fatty acid transport protein 1 and acyl-CoA synthase

- genes by dimer-selective rexinoids suggests that the peroxisome proliferator-activated receptor-retinoid X receptor heterodimer is its molecular target. *J Biol Chem* 275:12612–12618
47. Tontonoz P, Hu E, Devine J, Beale EG, Spiegelman BM 1995 PPAR γ 2 regulates adipose expression of the phosphoenolpyruvate carboxylase gene. *Mol Cell Biol* 15:351–357
 48. Magana MM, Lin SS, Dooley KA, Osborne TF 1997 Sterol regulation of acetyl coenzyme A carboxylase promoter requires two interdependent binding sites for sterol regulatory element binding proteins. *J Lipid Res* 38:1630–1638
 49. Schadinger SE, Bucher NL, Schreiber BM, Farmer SR 2005 PPAR γ 2 regulates lipogenesis and lipid accumulation in steatotic hepatocytes. *Am J Physiol Endocrinol Metab* 288:E1195–E1205
 50. Tontonoz P, Kim JB, Graves RA, Spiegelman BM 1993 ADD1: a novel helix-loop-helix transcription factor associated with adipocyte determination and differentiation. *Mol Cell Biol* 13:4753–4759
 51. Kim JB, Spiegelman BM 1996 ADD1/SREBP1 promotes adipocyte differentiation and gene expression linked to fatty acid metabolism. *Genes Dev* 10:1096–1107
 52. Joseph SB, Laffitte BA, Patel PH, Watson MA, Matsu-kuma KE, Walczak R, Collins JL, Osborne TF, Tontonoz P 2002 Direct and indirect mechanisms for regulation of fatty acid synthase gene expression by liver X receptors. *J Biol Chem* 277:11019–11025
 53. Seo JB, Moon HM, Kim WS, Lee YS, Jeong HW, Yoo EJ, Ham J, Kang H, Park MG, Steffensen KR, Stulnig TM, Gustafsson JA, Park SD, Kim JB 2004 Activated liver X receptors stimulate adipocyte differentiation through induction of peroxisome proliferator-activated receptor γ expression. *Mol Cell Biol* 24:3430–3444
 54. Yu S, Matsusue K, Kashireddy P, Cao WQ, Yeldandi V, Yeldandi AV, Rao MS, Gonzalez FJ, Reddy JK 2003 Adipocyte-specific gene expression and adipogenic steatosis in the mouse liver due to peroxisome proliferator-activated receptor γ 1 (PPAR γ 1) overexpression. *J Biol Chem* 278:498–505
 55. Hallakou S, Doare L, Foufelle F, Kergoat M, Guerre-Millo M, Berthault MF, Dugail I, Morin J, Auwerx J, Ferre P 1997 Pioglitazone induces in vivo adipocyte differentiation in the obese Zucker fa/fa rat. *Diabetes* 46:1393–1399
 56. de Souza CJ, Eckhardt M, Gagen K, Dong M, Chen W, Laurent D, Burkey BF 2001 Effects of pioglitazone on adipose tissue remodeling within the setting of obesity and insulin resistance. *Diabetes* 50:1863–1871
 57. Smith SR, De Jonge L, Volaufova J, Li Y, Xie H, Bray GA 2005 Effect of pioglitazone on body composition and energy expenditure: a randomized controlled trial. *Metabolism* 54:24–32
 58. Auwerx J 1999 PPAR γ , the ultimate thrifty gene. *Diabetologia* 42:1033–1049
 59. Ferre P 2004 The biology of peroxisome proliferator-activated receptors: relationship with lipid metabolism and insulin sensitivity. *Diabetes* 53(Suppl 1):S43–S50
 60. Day C 1999 Thiazolidinediones: a new class of antidiabetic drugs. *Diabet Med* 16:179–192
 61. Mukherjee R, Davies PJ, Crombie DL, Bischoff ED, Cesario RM, Jow L, Hamann LG, Boehm MF, Mondon CE, Nadzan AM, Paterniti Jr JR, Heyman RA 1997 Sensitization of diabetic and obese mice to insulin by retinoid X receptor agonists. *Nature* 386:407–410
 62. Hill JO, Peters JC 1998 Environmental contributions to the obesity epidemic. *Science* 280:1371–1374
 63. Barker DJ, Bull AR, Osmond C, Simmonds SJ 1990 Fetal and placental size and risk of hypertension in adult life. *Br Med J* 301:259–262
 64. Phillips DI, Hirst S, Clark PM, Hales CN, Osmond C 1994 Fetal growth and insulin secretion in adult life. *Diabetologia* 37:592–596
 65. Martyn CN, Barker DJ, Jespersen S, Greenwald S, Osmond C, Berry C 1995 Growth in utero, adult blood pressure, and arterial compliance. *Br Heart J* 73:116–121
 66. Yajnik C 2000 Interactions of perturbations in intrauterine growth and growth during childhood on the risk of adult-onset disease. *Proc Nutr Soc* 59:257–265
 67. Barker DJ, Martyn CN, Osmond C, Hales CN, Fall CH 1993 Growth in utero and serum cholesterol concentrations in adult life. *Br Med J* 307:1524–1527
 68. Lucas A 1998 Programming by early nutrition: an experimental approach. *J Nutr* 128:401S–406S
 69. Armitage JA, Khan IY, Taylor PD, Nathanielsz PW, Poston L 2004 Developmental programming of metabolic syndrome by maternal nutritional imbalance; how strong is the evidence from experimental models in mammals? *J Physiol* 561:355–377
 70. Masuno H, Kidani T, Sekiya K, Sakayama K, Shiosaka T, Yamamoto H, Honda K 2002 Bisphenol A in combination with insulin can accelerate the conversion of 3T3-L1 fibroblasts to adipocytes. *J Lipid Res* 43:676–684
 71. Masuno H, Okamoto S, Iwanami J, Honda K, Shiosaka T, Kidani T, Sakayama K, Yamamoto H 2003 Effect of 4-nonylphenol on cell proliferation and adipocyte formation in cultures of fully differentiated 3T3-L1 cells. *Toxicol Sci* 75:314–320
 72. Toschke AM, Koletzko B, Slikker Jr W, Hermann M, von Kries R 2002 Childhood obesity is associated with maternal smoking in pregnancy. *Eur J Pediatr* 161:445–448
 73. von Kries R, Toschke AM, Koletzko B, Slikker Jr W 2002 Maternal smoking during pregnancy and childhood obesity. *Am J Epidemiol* 156:954–961
 74. Oken E, Huh SY, Taveras EM, Rich-Edwards JW, Gillman MW 2005 Associations of maternal prenatal smoking with child adiposity and blood pressure. *Obes Res* 13:2021–2028
 75. Power C, Jefferis BJ 2002 Fetal environment and subsequent obesity: a study of maternal smoking. *Int J Epidemiol* 31:413–419
 76. Hill SY, Shen S, Locke Wellman J, Rickin E, Lowers L 2005 Offspring from families at high risk for alcohol dependence: increased body mass index in association with prenatal exposure to cigarettes but not alcohol. *Psychiatry Res* 135:203–216
 77. Umesonon K, Murakami KK, Thompson CC, Evans RM 1991 Direct repeats as selective response elements for the thyroid hormone, retinoic acid, and vitamin D3 receptors. *Cell* 65:1255–1266
 78. Perlmann T, Rangarajan PN, Umesonon K, Evans RM 1993 Determinants for selective RAR and TR recognition of direct repeat HREs. *Genes Dev* 7:1411–1422
 79. Blumberg B, Mangelsdorf DJ, Dyck JA, Bittner DA, Evans RM, De Robertis EM 1992 Multiple retinoid-responsive receptors in a single cell: families of retinoid “X” receptors and retinoic acid receptors in the *Xenopus* egg. *Proc Natl Acad Sci USA* 89:2321–2325
 80. Blumberg B, Bolado J Jr, Derguini F, Craig AG, Moreno TA, Chakravarti D, Heyman RA, Buck J, Evans RM 1996 Novel retinoic acid receptor ligands in *Xenopus* embryos. *Proc Natl Acad Sci USA* 93:4873–4878
 81. Blumberg B, Sabbagh Jr W, Juguilon H, Bolado Jr J, van Meter CM, Ong ES, Evans RM 1998 SXR, a novel steroid and xenobiotic-sensing nuclear receptor. *Genes Dev* 12:3195–3205
 82. Tabb MM, Sun A, Zhou C, Grun F, Errandi J, Romero K, Pham H, Inoue S, Mallick S, Lin M, Forman BM, Blumberg B 2003 Vitamin K2 regulation of bone homeostasis is mediated by the steroid and xenobiotic receptor SXR. *J Biol Chem* 278:43919–43927
 83. Grun F, Blumberg B 2003 Identification of novel nuclear hormone receptor ligands by activity-guided purification. *Methods Enzymol* 364:3–24
 84. Grun F, Venkatesan RN, Tabb MM, Zhou C, Cao J, Hemmati D, Blumberg B 2002 Benzoate X receptors α

- and β are pharmacologically distinct and do not function as xenobiotic receptors. *J Biol Chem* 277:43691–43697
85. Livak KJ, Schmittgen TD 2001 Analysis of relative gene expression data using real-time quantitative PCR and the $2^{-\Delta\Delta C(T)}$ method. *Methods* 25:402–408
86. Bourguet W, Ruff M, Chambon P, Gronemeyer H, Moras D 1995 Crystal structure of the ligand-binding domain of the human nuclear receptor RXR- α . *Nature* 375:377–382
87. Allegretto EA, McClurg MR, Lazarchik SB, Clemm DL, Kerner SA, Elgort MG, Boehm MF, White SK, Pike JW, Heyman RA 1993 Transactivation properties of retinoic acid and retinoid X receptors in mammalian cells and yeast. Correlation with hormone binding and effects of metabolism. *J Biol Chem* 268:26625–26633
88. Lehmann JM, Moore LB, Smith-Oliver TA, Willkison WO, Willson TM, Kliewer SA 1995 An antidiabetic thiazolidinedione is a high affinity ligand for peroxisome proliferator-activated receptor γ (PPAR γ). *J Biol Chem* 270:12953–12956
89. Nieuwkoop P, Faber J 1994 Normal table of *Xenopus laevis* (Daudin). 2nd ed. New York: Garland Publishing, Inc.
90. Rugh R 1962 Experimental embryology: techniques and procedures. 3rd ed. Minneapolis: Burgess Publishing Co.



Molecular Endocrinology is published monthly by The Endocrine Society (<http://www.endo-society.org>), the foremost professional society serving the endocrine community.

Tbx6-mediated Notch signaling controls somite-specific *Mesp2* expression

Yukuto Yasuhiko*, Seiki Haraguchi†, Satoshi Kitajima*, Yu Takahashi*, Jun Kanno*, and Yumiko Saga*[§]

*Cellular and Molecular Toxicology Division, National Institute of Health Sciences, Kamiyoga 1-18-1, Setagaya-ku, Tokyo 158-8501, Japan; †The Wellcome Trust/Cancer Research UK Gurdon Institute, University of Cambridge, Cambridge CB2 1QN, United Kingdom; and [§]Division of Mammalian Development, National Institute of Genetics, Mishima, Shizuoka 411-8540, Japan

Edited by Kathryn V. Anderson, Sloan-Kettering Institute, New York, NY, and approved January 10, 2006 (received for review September 21, 2005)

Mesp2 is a transcription factor that plays fundamental roles in somitogenesis, and its expression is strictly restricted to the anterior presomitic mesoderm just before segment border formation. The transcriptional on-off cycle is linked to the segmentation clock. In our current study, we show that a T-box transcription factor, Tbx6, is essential for *Mesp2* expression. Tbx6 directly binds to the *Mesp2* gene upstream region and mediates Notch signaling, and subsequent *Mesp2* transcription, in the anterior presomitic mesoderm. Our data therefore reveal that a mechanism, via Tbx6-dependent Notch signaling, acts on the transcriptional regulation of *Mesp2*. This finding uncovers an additional component of the interacting network of various signaling pathways that are involved in somitogenesis.

enhancer | transgenic mouse | RBPJ κ | luciferase assay

Somitogenesis not only is an important morphogenic process that generates metamer structures in vertebrates, but it is also a intriguing model system for the study of the interactions among various signaling cascades that facilitate periodic pattern formation. The segmental boundary of each somite forms at the anterior end of the presomitic mesoderm (PSM) or unsegmented paraxial mesoderm, which is supplied from the primitive streak or tailbud at a later stage of development.

Notch signaling plays fundamental roles in segmental pattern formation by means of oscillating the activity in the tailbud, its forward movement through the PSM as traveling waves, and its stabilization at the anterior end of the PSM (1, 2). A segment border forms at the posterior limit of the stabilized stripe of Notch signaling activity (2). The oscillation of the Notch signals in the tailbud region is regulated by the transcription factor *Hes7* (3), a glycosyltransferase *Lunatic fringe* (2), and by Wnt signaling (4). In contrast, the positioning of segment formation by a determination wavefront is thought to be defined by antagonistic interactions between gradients of Fgf signals from the posterior end (5) and retinoic acid (RA) from anterior end of the PSM (6). On the other hand, mutant analyses identified a T-box protein, Tbx6, as an indispensable component for correct PSM differentiation and segmentation (7). However, the direct molecular relationships between these factors have not yet been well characterized.

A basic helix-loop-helix transcription factor, *Mesp2*, has a crucial role both in somite segment border formation and in the establishment of the rostrocaudal patterning of each somite (8). *Mesp2* shows dynamic and periodical expression in the anterior PSM, which defines the positioning of the forming somite by suppressing Notch signaling, partly through the activation of *lunatic fringe* (2). Genetic analyses have revealed that *Mesp2* expression itself is controlled by Notch signaling, which indicates the presence of a complicated feedback circuitry (9, 10). However, the molecular mechanisms that control *Mesp2* expression remain largely unknown. In our present study, we show that Tbx6 directly binds to upstream elements of the *Mesp2* gene and is essential for the activation of *Mesp2* expression. Furthermore, we demonstrate that Notch signaling strongly enhances *Mesp2* ac-

tivation by Tbx6, and we identify the sequences that are important for this enhancement. Hence, we identify a Tbx6-mediated Notch signaling pathway as a mechanism underlying the regulation of *Mesp2* expression.

Results and Discussion

Evolutionally Conserved Sites in the Upstream Region of the *Mesp2* Gene Promote Strong Reporter Activity in Forming Somites. The distinct expression patterns of *Mesp2* expression during somitogenesis are strictly regulated. As we previously reported (11), a transgenic approach has revealed that a 300-bp portion of the 5'-adjoining sequence of the *Mesp2* ORF induces lacZ reporter activity in forming somites. This finding reflects the *Mesp2* expression pattern in the anteriormost PSM, suggesting that this 5' region includes cis elements that regulate PSM-specific *Mesp2* expression. We performed comparisons of the genomic sequences of mouse *Mesp2* and its putative ortholog in zebrafish, *mespb*, and identified five conserved sites (A–E) in this 300-bp segment (Fig. 1A). Each of these sites was then independently examined for enhancer properties by using a transgenic strategy. We previously showed that one of our transgenic constructs, *P2L-100*, containing sites D and E, which cover the 100 bp upstream of the *Mesp2* ATG start codon, did not activate the lacZ reporter gene (11). We thus concentrated our analysis on sites A–C in our current experiments by ligating them with the *P2L-100* construct. None of these three sites could individually promote lacZ reporter activity in somites (Fig. 1B). However, the combination of sites A and B (designated as “site A+B” hereafter) induced strong β -gal expression in the somite region (Fig. 1B Left). This result suggests that specific transcription factors required for somite-specific *Mesp2* expression may bind to site A+B.

Tbx6 Binds to Cis-Regulatory Elements of the *Mesp2* Gene and Activates Its Expression. To identify transcription factors that bind to the cis-regulatory elements of the *Mesp2* gene, we performed yeast one-hybrid screening. Using site A+B sequences as the “bait,” we isolated a T-box transcription factor, Tbx6, as a candidate binding protein. T-box proteins have been shown to recognize and bind to nucleotide sequences of 10–11 bp in length that possess a conserved CACAC motif (12). Significantly, sites A, B, and D in the upstream sequences of the *Mesp2* gene contain this motif (Fig. 2A). EMSA subsequently revealed that FLAG-Tbx6 binds to both site B and site D, in addition to the T (Brachyury) binding consensus sequence (12) (Fig. 6A, which is published as supporting information on the PNAS web site). By using site B sequences as a probe for FLAG-Tbx6 binding, EMSA experiments produced two band shifts, a distinct band

Conflict of interest statement: No conflicts declared.

This paper was submitted directly (Track II) to the PNAS office.

Abbreviations: PSM, presomitic mesoderm; NICD, Notch intracellular domain; RA, retinoic acid.

[§]To whom correspondence should be addressed. E-mail: ysaga@lab.nig.ac.jp.

© 2006 by The National Academy of Sciences of the USA

To examine the function of these upstream *Mesp2* cis elements on gene expression, we performed transient transgenic mouse analyses using a lacZ reporter with mutated cis elements in 6-kb upstream sequences of the *Mesp2* ORF. The nucleotide substitutions that eliminate the binding of Tbx6 to sites B and D of the *Mesp2* promoter (P2EmB1D) diminished gene reporter activity in these assays (Fig. 2C). Furthermore, targeted disruption of sites B and D eliminated *Mesp2* expression in the forming somites of homozygous embryos (data not shown), demonstrating that these cis-regulatory elements are essential for somite-specific *Mesp2* expression.

In mouse embryo, *Mesp2* mRNA emerges in anterior PSM, at the position of S-1 (8, 9). Tbx6 protein exists also in S-1 (20). *Mesp2* is not expressed in the PSM of *Tbx6*-null mouse embryos (7), suggesting that it is a downstream target of Tbx6. Although the distinct *Mesp2* signal overlaps only in the anteriormost part of *Tbx6*, the initial *Mesp2* mRNA emerges in the more posterior region, overlapping with the *Tbx6* signal (Fig. 6E). These results suggest that Tbx6 is necessary at least for initiation of *Mesp2* expression.

In zebrafish, *fused somite (fss)*, which encodes *Tbx24*, is known as a distant homolog of mouse *Tbx6*, and the corresponding mutant embryos have neither segmented somite nor *mespb* expression (21). The cis-regulatory elements are also well conserved between the upstream regions of *Mesp2* and *mespb* (Fig. 1A), and *Tbx24* also binds to the *Mesp2* upstream region (data not shown). Recently, Davidson *et al.* (22) reported that, during heart development in the simple chordate *Ciona intestinalis*, a *Mesp* homolog is also expressed in a Tbx6-dependent manner. Comparing genomic sequences among *Ciona*, mouse, and zebrafish, the authors identified multiple Tbx6 binding sites in the upstream sequence of *Ciona Mesp* homolog. Taken together, we speculate from these findings that Tbx6-mediated activation of the *Mesp* genes is an evolutionally conserved mechanism in Chordata.

The Notch Intracellular Domain (NICD) Activates a *Mesp2* Reporter Construct in a Tbx6-Dependent Manner. To analyze the detailed regulatory mechanisms underlying the control of *Mesp2* expression, we constructed a *Mesp2* reporter system comprising a firefly luciferase reporter and *Mesp2* cis elements. Cotransfection of a Tbx6 expression vector with the *Mesp2* reporter increased luciferase activity by 10-fold (Fig. 3), indicating that Tbx6 functions as a transcriptional activator of *Mesp2*. In somite-stage embryos, *Tbx6* is expressed throughout the PSM and also in the tailbud region (20, 23), whereas *Mesp2* expression is restricted to the anterior PSM just before somite formation, and the expression overlaps only in the anterior limit of the *Tbx6* expression domain (Fig. 6E). The discrepancy between these expression patterns strongly indicates that other unknown factor(s) participate in the pathways that restrict the *Mesp2* expression domain to the anterior PSM. Because Notch signaling plays crucial roles in many aspects of somitogenesis, and given that *Mesp2* expression is known to depend on Dll1-Notch signaling (10), we examined the involvement of Notch signaling in the Tbx6-mediated transactivation of *Mesp2*.

The typical Notch signaling pathway is composed of ligands known as DSL (Delta, Serrate, and Lag-2), Notch receptors, effectors known as CSL (CBF-1, Suppressor of Hairless, and Lag-1), and a number of other proteins that modulate the functions of each component of the pathway (24). Once the DSL ligands bind to the Notch receptor, the NICD is proteolytically cleaved, translocates into the nucleus, and binds to its CSL effector (RBPJ κ in the case of mouse) to activate the transcription of downstream target genes (24). We transiently introduced expression vectors for NICD and RBPJ κ -VP16 (dominant-active RBPJ κ) (25), in conjunction with Tbx6, into cultured cells bearing the *Mesp2* reporter. As a positive control, we used the

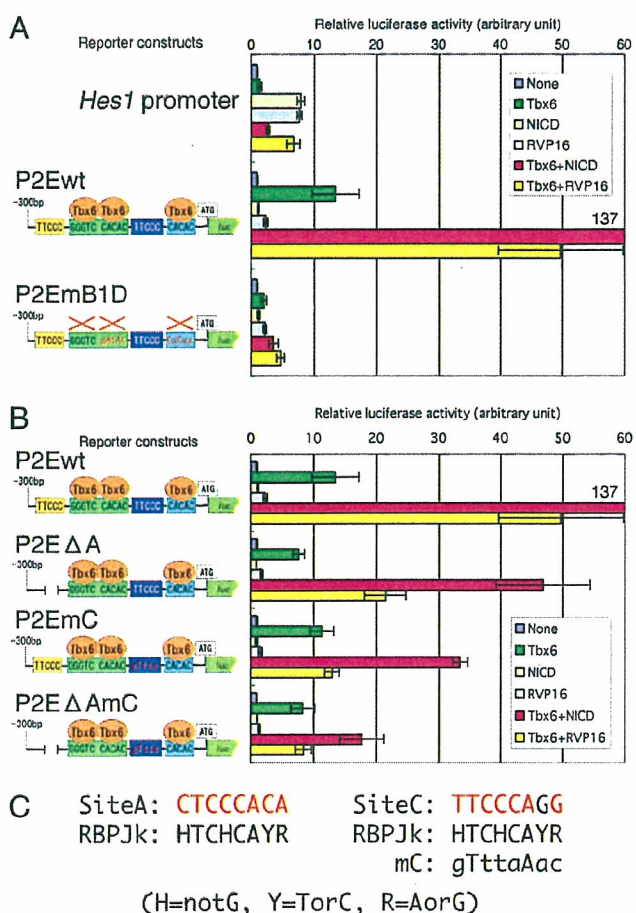


Fig. 3. *Mesp2* expression is activated by Notch signaling in a Tbx6-dependent manner. For each set of analyses, the luciferase activity was normalized to the values obtained in the absence of an expression vector (None). Error bars represent the standard deviation from six independent experiments. RVP16, RBPJ κ -VP16. (A) Tbx6 activates a *Mesp2*-luciferase reporter gene construct synergistically with the NICD or RBPJ κ -VP16. Mutation of site B and site D (denoted as P2EmB1D) eliminates this transactivation. (B) Notch signal activates the *Mesp2* reporter construct via site A and site C. The reporter constructs are indicated to the left of the graph. (C) Nucleotide sequences of the possible RBPJ κ binding sites in site A (Left) and site C (Right) and the comparison between these regions and the RBPJ κ binding consensus sequence (denoted as RBPJ κ) (27). The nucleotides matching the consensus sequence are shown in red for site A and site C. Nucleotide substitutions in site C (denoted as mC) are indicated in lowercase.

Hes1 promoter, which is known to be a downstream target of Notch signaling (26). Transfection of the *Hes1* reporter construct produced significant luciferase activity even in the absence of NICD (data not shown), reflecting the endogenous NICD activity, and the reporter activity increased further in the presence of either NICD or RBPJ κ -VP16. In contrast, neither NICD nor RBPJ κ -VP16 was found to activate the *Mesp2* reporter (Fig. 3A). However, when NICD and Tbx6 were cotransfected, significant increases in luciferase activity were detected (Fig. 3A). RBPJ κ -VP16 also can activate the *Mesp2* promoter when cotransfected with *Tbx6* (Fig. 3A), suggesting that RBPJ κ -dependent Notch signaling activated *Mesp2* reporter in a Tbx6-dependent manner. Consistent with this finding, mutations in site B and site D, which eliminate Tbx6 binding to the *Mesp2* upstream region, greatly reduced *Mesp2* reporter activation by NICD or RBPJ κ -VP16 (Fig. 3A).

To identify the Notch signaling responsive site within the

Mesp2 upstream region, we analyzed the activity of two additional reporter constructs bearing either a deletion or a mutation in the conserved sites A and C, because these regions contain sequences that have some similarity to the RBPJ κ consensus binding site (24, 27) (Fig. 3C). We speculated that these sites may play an important role in the regulation of *Mesp2* expression based on our observation that site A is essential for somite-specific expression in combination with site B (Fig. 1). Moreover, reporter activity in forming somites is lost when sequential deletion of the upstream region of the *Mesp2* gene removes a part of site C (11). In our current experiments, the deletion of site A reduced the levels of synergistic activation of the *Mesp2* reporter by both Notch signaling and Tbx6 by up to 50% (Fig. 3B, P2E Δ A). Reporter activation was also remarkably diminished when we introduced mutations into both site A and site C (Fig. 3B, P2E Δ AmC), suggesting that the binding of RBPJ κ is required for the Tbx6-dependent transduction of Notch signaling. In contrast to the *Hes* family genes, no direct interaction between the Notch signaling pathway and the *Mesp2* regulatory region had been previously identified. Our current findings thus provide the first evidence that *Mesp2* is a direct target of Notch signaling. Furthermore, we identified a regulatory mechanism underlying the Notch signaling pathway that is based on the binding of Tbx6 to transcriptional regulatory sequences (summarized in Fig. 4A and B).

We next conducted transient transgenic assays using our lacZ reporters with mutations in sites A and C. Surprisingly, the coexistence of the site A deletion and site C mutation (P2E Δ AmC) in our reporter system showed somite-specific β -gal expression, although the activity was slightly weaker than normal (Fig. 5A). One possibility that might explain this disparity is that there may be a redundant, RBPJ κ -independent pathway of Notch signaling that activates *Mesp2* expression. Consistent with this hypothesis, the P2E Δ AmC reporter retained the ability to respond to the coexpression of NICD and Tbx6, although this activity was only 13% of wild-type levels (Fig. 3B). Notably, the P2E Δ AmC reporter showed no synergistic activation after the coexpression of Tbx6 and RBPJ κ -VP16 (Fig. 3B), indicating that the ability to respond to RBPJ κ -dependent Notch signaling is eliminated by the disruption of sites A and C. These results suggest that Notch signaling activates *Mesp2* expression in both RBPJ κ -dependent and RBPJ κ -independent manners (Fig. 4C). Although most of the Notch signals are mediated by CSL effectors, such as RBPJ κ , there is some reported evidence that suggests the existence of RBPJ κ -independent Notch signal transduction pathways (28, 29). The molecular components involved in RBPJ κ -independent Notch signaling are still poorly understood, but our present data suggest the possibility that Tbx6 not only facilitates RBPJ κ -dependent Notch signaling but also acts as a component of an RBPJ κ -independent Notch signaling pathway.

Another possible mechanism of somite-specific reporter expression that we observed in our P2E Δ AmC transgenic embryos is the involvement of Notch-independent signals (Fig. 4C). Although it is clear that Notch signaling is genetically upstream of *Mesp2* activation (9, 10), *Psen1* knockout mouse embryos, which are deficient in Notch proteolysis and therefore do not produce NICD (30), show only moderate decreases in *Mesp2* expression levels (10). Together with our present findings, these observations may indicate that the controlling mechanism for *Mesp2* gene expression is a redundant and robust system and is composed of a number of signaling cascades. Regardless of this possibility, Tbx6 is likely to be essential for all of the signaling pathways involved in *Mesp2* expression, because mutation of the Tbx6 binding sites in the upstream regions of the *Mesp2* gene completely eliminates reporter expression in forming somites (Fig. 2C).

Because Tbx6 mRNA (Fig. 6E) and protein (20) are distrib-

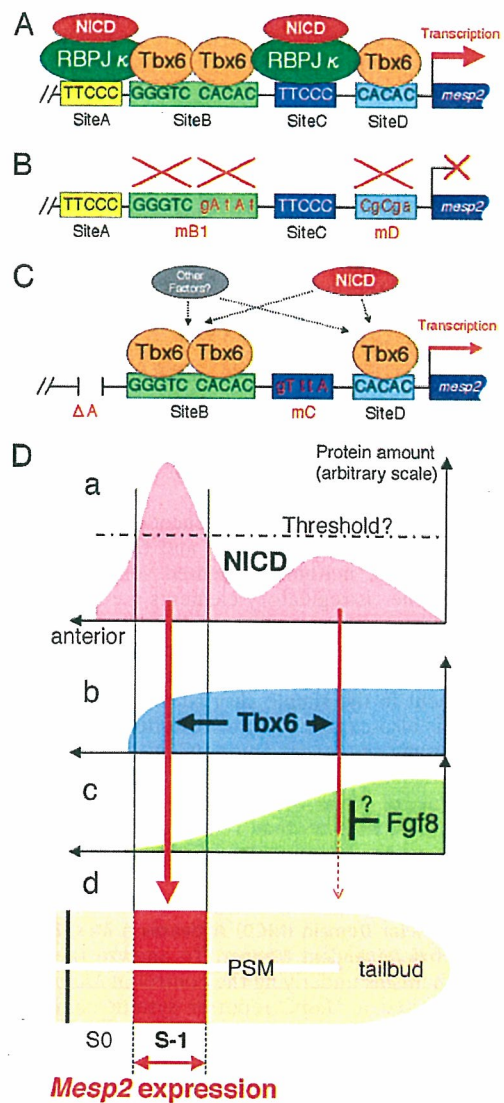


Fig. 4. Proposed mechanisms underlying the control of *Mesp2* expression. Tbx6 and NICD (colored ovals) interact with the conserved upstream sites in the *Mesp2* gene, sites A–D (represented by boxes). Tbx6 binds to site B (two molecules) and site D (single molecule). Site A and site C interact with RBPJ κ to achieve a significant increase in *Mesp2* expression levels in the presence of Notch signals (A). This activation fully depends on the binding of Tbx6 to site B or site D (B). Tbx6 may activate *Mesp2* expression without site A and site C, presumably through an RBPJ κ -independent Notch signaling pathway and via other signals (C). (D) Schematic representation of a proposed model that may explain developmentally regulated *Mesp2* expression in the anterior PSM. (a) NICD is highly accumulated in the anterior PSM and less in the posterior (1, 2) to activate *Mesp2* expression (red arrows). There may be a threshold level of NICD accumulation to initiate *Mesp2* activation (broken line). (b) Tbx6 protein is distributed in the tailbud and PSM (20) and facilitates *Mesp2* activation by NICD. (c) It is possible that the activation of *Mesp2* expression in the tailbud and posterior PSM, if any, is repressed by other factor(s), such as Fgf8 (36), via an unknown mechanism. (d) As a result, *Mesp2* expression is restricted in the anterior PSM (red box).

uted throughout the tailbud and posterior PSM, the factors that restrict the expression domain of *Mesp2* in anterior PSM remain to be identified. Notably, although Tbx6 seems to activate reporter expression in cultured cells by itself, dominant-negative RBPJ κ (R218H), which retains NICD binding activity but has lost any DNA binding ability (31), inhibits the Tbx6-dependent reporter activation by 50% (Fig. 5B). This finding suggests that

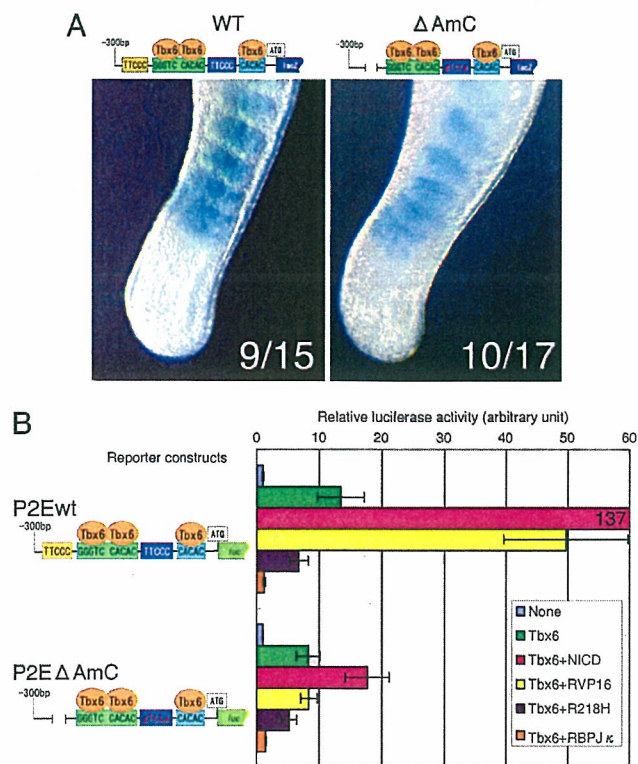


Fig. 5. The expression of *Mesp2* is not achieved solely by RBPJ κ -dependent Notch signaling. (A) Transgenic analyses reveal that somite-specific reporter expression can still be observed using the P2E Δ AmC construct, which contains a deletion of site A and mutations in site C. The numbers of β -gal-positive embryos are indicated for each image (β -gal-positive/transgene-positive). (B) The expression of a dominant-negative RBPJ κ diminishes reporter activation by Tbx6 for both the wild-type (wt) and P2E Δ AmC (Tbx6+R218H, purple bars) vectors. Wild-type RBPJ κ also strongly suppressed reporter activity driven by Tbx6 (Tbx6+RBPJ κ , orange bars). Error bars represent the standard deviation in six independent experiments.

Tbx6 itself has only weak transactivation properties, if any, and needs to cooperate with other signals such as Notch for full activity. We speculate that reporter activation by Tbx6 itself (Figs. 3 and 5) may be accomplished by cooperation with Notch signaling, presumably driven by endogenous NICD in cultured cells. Endogenous NICD concentration in cells or tissues is very low and biochemically undetectable (32). However, cultured fibroblast cells express mature Notch protein (33) and show γ -secretase-like activity that generates NICD from Notch protein (32). Furthermore, NICD activates *Hes1* reporter at very low concentrations, below the level of biochemical detection (32). Consistent with these data, *Hes1* reporter showed higher basal activity than *Mesp2* reporters or control reporter with no promoter/enhancer: 100 times higher in COS-7 cells and 60 times higher in NIH/3T3 cells in our observation (data not shown). We suppose that endogenous NICD affects the expression of Notch downstream genes in cultured cells.

NICD accumulation is observed as a strong band-like pattern in the anterior PSM and as a weak diffused signal in the posterior PSM (1, 2). *Mesp2* is initially detectable in the middle of a distinct band of NICD in the anterior PSM (2), consistent with the importance of Notch signaling in *Mesp2* expression indicated by our present study. However, the weak Notch signaling activity observed in the posterior PSM may activate *Mesp2* expression, whereas *Mesp2* transcripts appear only in the anterior PSM. One possibility is that there is a "threshold" of NICD levels that is

required to trigger Tbx6-dependent *Mesp2* activation (Fig. 4D). Because RBPJ κ is expressed ubiquitously in the developing embryo (34) and strongly represses Tbx6-dependent activation of the *Mesp2* reporters (Fig. 5B), it may also function as a suppressor in the posterior PSM that prevents inadequate expression of *Mesp2*.

Recent reports also indicate that there are two gradients of mutually inhibitory signals, Fgf8 and RA, that have important roles in the positional determination of segment formation (35). It is likely therefore that the Fgf8 and RA signals also participate in the regulation of *Mesp2* expression. Recently, Delfini *et al.* (36) reported an intriguing result suggesting that Fgf signaling represses *Mesp* expression. Using *in ovo* electroporation, they demonstrated that the up-regulation of Fgf in the PSM diminishes the endogenous expression of *cMeso*, the chick *Mesp* homolog. It is plausible therefore that Fgf8, which is strongly expressed in the tailbud and posterior PSM, prevents the inadequate expression of *Mesp2* in posterior region. The involvement of RA in *Mesp2* expression remains elusive, however, because the disruption of *CYP26* (37), a degradation enzyme for RA, does not severely affect *Mesp2* expression levels (2). In the zebrafish embryo, FGF signaling up-regulates a basic helix-loop-helix transcription factor, *her13.2*, which maintains the oscillation of the Notch signals in both the tailbud and PSM by repressing the Notch-regulated genes *her1* and *her7* (38). RA and Fgf signals may thus contribute to the positioning of *Mesp2* expression by coordinating the regular oscillation of Notch signals in the tailbud and PSM.

Interestingly, it has been revealed that *Tbx6* is one of the direct targets of RBPJ κ -dependent Notch signaling (39). During somitogenesis, Notch signals may first activate *Tbx6* expression in the tailbud and posterior PSM region and then activate *Mesp2* expression in the anterior PSM in cooperation with Tbx6. Furthermore, Tbx6 also works upstream of the Notch signaling pathway. In embryos of *Tbx6* hypomorphic mutant mice, *Dll1* expression in the tailbud and posterior PSM is greatly reduced (40). Promoter analyses of *Dll1* have demonstrated that Tbx6, in synergy with Wnt signaling, activates *Dll1* expression by binding to T-binding consensus sequences (20, 41). Taken together, our present results demonstrate that Tbx6 and Notch signaling constitute a regulatory network that controls somite formation via the regulation of *Mesp2* expression.

Materials and Methods

Transgenic Analyses. DNA fragments, with and without mutations in conserved upstream sites, were generated from a *Mesp2* genomic fragment by using a standard PCR-based protocol. Transgene inserts were digested from the corresponding plasmids, purified, and injected into the male pronucleus of a fertilized egg (42). The injected embryos were then transferred into pseudopregnant recipients and allowed to develop until 9.5–10.5 days postcoitum. Embryos were then analyzed for lacZ expression by X-gal staining (43) and subsequently examined for the presence of the transgene by PCR analysis (44).

Yeast One-Hybrid Screening. Synthetic oligonucleotides corresponding to contiguous sequences of conserved site A (nucleotides -199 to -191 from first ATG of *Mesp2* ORF) and site B (nucleotides -162 to -140) were inserted into the vectors pHISi-1 and placZi (Clontech), immediately upstream of the HIS3 and lacZ reporter genes, respectively. The resulting constructs were then linearized and introduced simultaneously into *Saccharomyces cerevisiae* YM4271 (Clontech) to generate the bait strain. The bait strain was then transformed by using 80 μ g of 11.5 days postcoitum mouse tail cDNA library plasmid (45) to screen up to 2 million independent clones. We obtained hundreds of positive clones (HIS3+ and LacZ+) and recovered

library plasmid from 77 of these. Fifty-one of these 77 clones were sequenced and found to encode Tbx6.

EMSA. The full-length Tbx6 ORF was obtained from the pACT-Tbx6 construct, which was isolated from the yeast one-hybrid screening. After ligation to a 3XFLAG tag (Sigma), the tagged Tbx6 insert was cloned into pCS2+ (46). *In vitro* transcription/translation was then performed with a TNT *in vitro* translation kit (Promega) following the manufacturer's protocol. Oligonucleotide probes were labeled with digoxigenin-11-dideoxy UTP by using recombinant TdT (Roche Diagnostics). Crude *in vitro* translated product (5 μ l) was subjected to EMSA as a protein sample. As a negative control, reticulocyte lysate without Tbx6 template was used. EMSA was performed by using the DIG Gel Shift Kit, 2nd Generation (Roche Diagnostics), following the manufacturer's protocol. The band shifts were detected by using LumiImager LAS-1000 (Fuji).

Luciferase Assay. Segments (356 bp) corresponding to the 5'-adjoining sequence of the *Mesp2* ORF, with and without mutations in the conserved binding sites, were subcloned into the pGL3-Basic (Promega) vector to generate luciferase reporter constructs. The expression vectors for the proteins to be assessed were constructed in the same way as that used in the EMSAs

described above. COS-7 cells were routinely and regularly passaged in DMEM supplemented with 10% FBS. Cells were seeded at 2.5×10^4 cells per well in 24-well plates, and, after 24 h of cultivation, they were transfected with a total of 350 ng of DNA containing the reporter plasmids and expression vectors for the proteins under analysis (50 ng of each expression vector and 200 ng of reporter construct, adjusted to 350 ng by the addition of empty vector). Twenty-four hours after transfection, the cells were lysed by Passive Lysis Buffer (Promega) and subjected to a luciferase assay by using the Dual Luciferase System (Promega). In all experiments, 5 ng of the sea pansy luciferase expression vector phRL-TK (Promega) was used per well as the internal control. Luciferase activity was normalized to the phRL-TK internal control activity (sea pansy luciferase). The experiments were performed in triplicate for each assay and repeated at least twice.

We are grateful to Tasuku Honjo (Kyoto University, Kyoto) for providing cDNA clones of RBPJ κ , RBPJ κ -VP16, and dnRBPJ κ (R218H) and to Mariko Ikumi, Eriko Ikeno, and Shinobu Watanabe for technical assistance. We also thank Hiroyuki Takeda, Mitsuru Morimoto, and Masayuki Oginuma for helpful discussions and for their comments on the manuscript. This work was supported by the Organized Research Combination System of the Ministry of Education, Culture, Sports, Science, and Technology, Japan.

- Huppert, S. S., Ilagan, M. X., De Strooper, B. & Kopan, R. (2005) *Dev. Cell* **8**, 677–688.
- Morimoto, M., Takahashi, Y., Endo, M. & Saga, Y. (2005) *Nature* **435**, 354–359.
- Bessho, Y., Hirata, H., Masamizu, Y. & Kageyama, R. (2003) *Genes Dev.* **17**, 1451–1456.
- Aulehla, A., Wehrle, C., Brand-Saberli, B., Kemler, R., Gossler, A., Kanzler, B. & Herrmann, B. G. (2003) *Dev. Cell* **4**, 395–406.
- Sawada, A., Shinya, M., Jiang, Y. J., Kawakami, A., Kuroiwa, A. & Takeda, H. (2001) *Development* **128**, 4873–4880.
- Moreno, T. A. & Kintner, C. (2004) *Dev. Cell* **6**, 205–218.
- Chapman, D. L. & Papaioannou, V. E. (1998) *Nature* **391**, 695–697.
- Saga, Y., Hata, N., Koseki, H. & Taketo, M. M. (1997) *Genes Dev.* **11**, 1827–1839.
- Takahashi, Y., Koizumi, K., Takagi, A., Kitajima, S., Inoue, T., Koseki, H. & Saga, Y. (2000) *Nat. Genet.* **25**, 390–396.
- Takahashi, Y., Inoue, T., Gossler, A. & Saga, Y. (2003) *Development* **130**, 4259–4268.
- Haraguchi, S., Kitajima, S., Takagi, A., Takeda, H., Inoue, T. & Saga, Y. (2001) *Mech. Dev.* **108**, 59–69.
- Conlon, F. L., Fairclough, L., Price, B. M., Casey, E. S. & Smith, J. C. (2001) *Development* **128**, 3749–3758.
- Mitani, Y., Takahashi, H. & Satoh, N. (2001) *Development* **128**, 3717–3728.
- Muller, C. W. & Herrmann, B. G. (1997) *Nature* **389**, 884–888.
- Wilson, V. & Conlon, F. L. (2002) *Genome Biol.* **3**, REVIEWS3008.
- Kraus, F., Haenig, B. & Kispert, A. (2001) *Mech. Dev.* **100**, 83–86.
- Koseki, H., Wallin, J., Wilting, J., Mizutani, Y., Kispert, A., Ebensperger, C., Herrmann, B. G., Christ, B. & Balling, R. (1993) *Development* **119**, 649–660.
- Hurlin, P. J., Steingrimsson, E., Copeland, N. G., Jenkins, N. A. & Eisenman, R. N. (1999) *EMBO J.* **18**, 7019–7028.
- Lardelli, M. (2003) *Dev. Genes Evol.* **213**, 519–522.
- White, P. H. & Chapman, D. L. (2005) *Genesis* **42**, 193–202.
- Nikaido, M., Kawakami, A., Sawada, A., Furutani-Seiki, M., Takeda, H. & Araki, K. (2002) *Nat. Genet.* **31**, 195–199.
- Davidson, B., Shi, W. & Levine, M. (2005) *Development* **132**, 4811–4818.
- Chapman, D. L., Agulnik, I., Hancock, S., Silver, L. M. & Papaioannou, V. E. (1996) *Dev. Biol.* **180**, 534–542.
- Mumm, J. S. & Kopan, R. (2000) *Dev. Biol.* **228**, 151–165.
- Furriols, M. & Bray, S. (2000) *Dev. Biol.* **227**, 520–532.
- Jarriault, S., Brou, C., Logeat, F., Schroeter, E. H., Kopan, R. & Israel, A. (1995) *Nature* **377**, 355–358.
- Barolo, S., Walker, R. G., Polyansky, A. D., Freschi, G., Keil, T. & Posakony, J. W. (2000) *Cell* **103**, 957–969.
- Matsuno, K., Go, M. J., Sun, X., Eastman, D. S. & Artavanis-Tsakonas, S. (1997) *Development* **124**, 4265–4273.
- Hori, K., Fostier, M., Ito, M., Fuwa, T. J., Go, M. J., Okano, H., Baron, M. & Matsuno, K. (2004) *Development* **131**, 5527–5537.
- Koizumi, K., Nakajima, M., Yuasa, S., Saga, Y., Sakai, T., Kuriyama, T., Shirasawa, T. & Koseki, H. (2001) *Development* **128**, 1391–1402.
- Kato, H., Taniguchi, Y., Kurooka, H., Minoguchi, S., Sakai, T., Nomura-Okazaki, S., Tamura, K. & Honjo, T. (1997) *Development* **124**, 4133–4141.
- Schroeter, E. H., Kisslinger, J. A. & Kopan, R. (1998) *Nature* **393**, 382–386.
- De Strooper, B., Annaert, W., Cupers, P., Saftig, P., Craessaerts, K., Mumm, J. S., Schroeter, E. H., Schrijvers, V., Wolfe, M. S., Ray, W. J., et al. (1999) *Nature* **398**, 518–522.
- Oka, C., Nakano, T., Wakeham, A., de la Pompa, J. L., Mori, C., Sakai, T., Okazaki, S., Kawachi, M., Shiota, K., Mak, T. W. & Honjo, T. (1995) *Development* **121**, 3291–3301.
- Dubrule, J. & Pourquie, O. (2004) *Development* **131**, 5783–5793.
- Delfini, M. C., Dubrule, J., Malapert, P., Chal, J. & Pourquie, O. (2005) *Proc. Natl. Acad. Sci. USA* **102**, 11343–11348.
- Sakai, Y., Meno, C., Fujii, H., Nishino, J., Shiratori, H., Sajoh, Y., Rossant, J. & Hamada, H. (2001) *Genes Dev.* **15**, 213–225.
- Kawamura, A., Koshida, S., Hijikata, H., Sakaguchi, T., Kondoh, H. & Takada, S. (2005) *Genes Dev.* **19**, 1156–1161.
- White, P. H., Farkas, D. R. & Chapman, D. L. (2005) *Genesis* **42**, 61–70.
- White, P. H., Farkas, D. R., McFadden, E. E. & Chapman, D. L. (2003) *Development* **130**, 1681–1690.
- Hofmann, M., Schuster-Gossler, K., Watabe-Rudolph, M., Aulehla, A., Herrmann, B. G. & Gossler, A. (2004) *Genes Dev.* **18**, 2712–2717.
- Hogan, B., Beddington, R., Costantini, F. & Lacy, E. (1994) *Manipulating the Mouse Embryo: A Laboratory Manual* (Cold Spring Harbor Lab. Press, Woodbury, NY).
- Saga, Y., Yagi, T., Ikawa, Y., Sakakura, T. & Aizawa, S. (1992) *Genes Dev.* **6**, 1821–1831.
- Sasaki, H. & Hogan, B. L. (1996) *Genes Cells* **1**, 59–72.
- Ohara, O., Nagase, T., Mitsui, G., Kohga, H., Kikuno, R., Hiraoka, S., Takahashi, Y., Kitajima, S., Saga, Y. & Koseki, H. (2002) *DNA Res.* **9**, 47–57.
- Rupp, R. A., Snider, L. & Weintraub, H. (1994) *Genes Dev.* **8**, 1311–1323.

Mesp1-Nonexpressing Cells Contribute to the Ventricular Cardiac Conduction System[†]

Satoshi Kitajima,^{1*} Sachiko Miyagawa-Tomita,² Tohru Inoue,³ Jun Kanno,¹ and Yumiko Saga^{4*}

Previous fate mapping analysis, using Cre recombinase driven by the *Mesp1* locus, revealed that *Mesp1* is expressed in almost all of the precursors of the cardiovascular system, including the endothelium, endocardium, myocardium, and epicardium. *Mesp1*-nonexpressing cells were found to be restricted to the outflow tract cushion and along the interventricular septum (IVS), which is a location that is suggestive of specialized cardiac conduction system (CCS). In our current study, we examined the identity of these IVS cells by using the pattern of β -galactosidase activity in *CCS-lacZ* mice. In addition, by crossing *Mesp1-Cre* and *floxed GFP reporter* mice with *CCS-lacZ* mice, we have calculated that approximately 20% of the ventricular CCS within the IVS corresponds to *Mesp1*-nonexpressing cells. These data suggest that the ventricular CCS is of heterocellular origin. Furthermore, we indicate a possibility that a population of the cells that contribute to the ventricular CCS might be distinguished at an early stage of development. *Developmental Dynamics* 235:395–402, 2006. © 2005 Wiley-Liss, Inc.

Key words: *Mesp1*; mesoderm; heart differentiation; cardiac conduction system; cell-lineage analysis

Accepted 30 September 2005

INTRODUCTION

The heart is the first functional organ to be formed during organogenesis, and cells that are destined to form cardiac mesoderm are induced both before and during gastrulation. The cells of the cardiac mesoderm invaginate through the primitive streak and migrate with the cranial mesoderm. The bilaterally symmetric cardiac precursors subsequently migrate and converge at the midline of the embryo to form the cardiac crescent, which

then forms a linear, single heart tube. The heart tube, formed by an outer myocardium and an inner endocardium, then undergoes rightward looping, which is lined by an acellular matrix (the cardiac jelly). The looped heart tube then undergoes septation to generate a mature, four-chambered cardiac structure in mammals.

The heart is composed of three major cardiac cell types: (1) the endocardium, a part of which forms the cushion tissue by transformation from

epithelial to mesenchymal cells; (2) the myocardium; and (3) the epicardium (for review, see Moorman and Christoffels, 2003). The major components of the heart, such as endocardium and myocardium, are of mesodermal origin (i.e., cardiogenic mesoderm), but the contribution of other cell lineages has also been reported for both chick and mouse. Fate mapping of the avian cardiac neural crest has been well documented, and it was reported previously from such

The Supplementary Material referred to in this article can be found at <http://www.interscience.wiley.com/jpages/1058-8388/suppmat>

[†] This article was accepted for inclusion in *Developmental Dynamics* 235#1, January 2006—Cardiovascular Special Issue.

¹ Division of Cellular & Molecular Toxicology, Biological Safety Research Center, National Institute of Health Sciences, Setagaya-ku, Tokyo, Japan

² Department of Pediatric Cardiology, The Heart Institute of Japan, Tokyo Women's Medical University, Shinjuku-ku, Tokyo, Japan

³ Biological Safety Research Center, National Institute of Health Sciences, Setagaya-ku, Tokyo, Japan

⁴ Division of Mammalian Development, National Institute of Genetics, Mishima, Japan

Grant sponsor: Ministry of Education, Science, Sports, and Culture in Japan; Grant sponsor: Burroughs–Wellcome Fund Clinical Scientist Award in Translational Research.

*Correspondence to: Yumiko Saga, Ph.D., Division of Mammalian Development, National Institute of Genetics, Yata 1111, Mishima 411-8540, Japan. E-mail: ysaga@lab.nig.ac.jp or Satoshi Kitajima, D.V.M.Ph.D, Division of Cellular & Molecular Toxicology National Institute of Health Sciences, 1-18-1 Kamiyohga, Setagaya-ku, Tokyo 158-8501, Japan. E-mail: satoshi@nihs.go.jp

DOI 10.1002/dvdy.20640

Published online 29 November 2005 in Wiley InterScience (www.interscience.wiley.com).

experiments using quail–chick chimera that two types of mesenchyme, cardiac neural crest derived and non-neural crest derived, participate in outflow septation and remodeling (Kirby et al., 1983; Waldo et al., 1998). Recently, through the use of the *Cre-loxP* system in mice, it has been demonstrated clearly that the cardiac outflow tract (OT) cushions are contributed in part by cardiac neural crest cells (Yamauchi et al., 1999; Jiang et al., 2000). Additionally, lineage analysis using *Tie2-cre* in mice has suggested that the OT cushions are of mixed origins, containing neural crest cells and endocardium, whereas the atrioventricular (AV) cushions are mainly derived from cells originating from endocardium (Kisanuki et al., 2001).

The specialized cardiac conduction system (CCS) includes the sinoatrial (SA) node, which generates a pacemaker impulse; the AV node, which delays the electrical impulse and allows for the sequential contraction of the atrial and ventricular chambers of the heart; and the ventricular CCS, such as the atrioventricular bundle (AVB), bundle branches, and their ramifications, which facilitates the fast and coordinated conduction of impulses to and throughout the ventricles. Cells in the CCS are characterized by their larger size, reduced number of myofibrils, and large accumulations of glycogen (Mikawa, 1999). It has also been suggested that the CCS might be categorized into two parts based on their origin (Moorman et al., 1998, 2003). One is the SA and AV nodes, which might be derived from the slow-conducting myocardium of the inflow tract and AV canal. The other one is the ventricular CCS, which possibly develops from the trabecular ventricular component. In chick, an elegant series of experiments using retroviral lineage-tracing has provided strong evidence that ventricular components of the conduction system are derived from cardiomyogenic cells (Gourdie et al., 1995; Cheng et al., 1999). In addition, it has been suggested that the differentiation of a subset of Purkinje fibers, adjacent to the arterial bed, might be regulated by local signals from the coronary artery (Gourdie et al., 1995). It was subsequently shown that endo-

thelin-1, a paracrine factor secreted by endothelial cells, is capable of inducing embryonic chick myocytes to the cells of the CCS.

In contrast to the avian CCS, the ventricular CCS in most mammals is morphologically and topologically different from that of chick as it is mainly subendocardial. Hence, the developmental role of the coronary artery in mammalian CCS differentiation is uncertain. In the murine heart, the expression of several markers, including specific connexins and *lacZ* under the transcriptional regulation of either the *minK* or *HF-1b* loci, delineate the bundle branches and proximal Purkinje fibers, but none appear to delineate the full extent of the conductive network along the ventricular free walls (Delorme et al., 1995; Copen et al., 1998, 1999; Kupershmidt et al., 1999; Nguyen-Tran et al., 2000). In contrast, the entire mouse CCS, including the distal Purkinje fiber network, in both embryonic and neonatal hearts has been visualized recently by way of β -galactosidase (β -gal) reporter activity (Rentschler et al., 2001) in the *CCS-lacZ* mouse line. Recently, the β -gal-positive cells in the interventricular septum (IVS) region of the *CCS-lacZ* adult mice have been reported to correspond to the Cx40-positive cells (Myers and Fishman, 2004). However, the comparison was performed by using serial sections; thus, further clarification is needed to determine whether the same cell expresses the both markers or not. Nevertheless, it is considered that the β -gal-positive cells of *CCS-lacZ* embryos are the most reliable indication for CCS cells in the mouse embryo, compared with the other markers. Although the lineage of the cells of the murine CCS is incompletely characterized, a recent study demonstrated that exogenous treatment of 8.5–10.5 days postcoitum (dpc) embryos with neuregulin-1, an endocardial-derived growth and differentiation factor essential for ventricular trabeculation, could induce a CCS-like phenotype in embryonic cardiomyocytes (Rentschler et al., 2002). Whereas, the use of in vitro culture systems has demonstrated also that the treatment of embryonic stem cells with endothelin-1 but not with neuregulin-1 increased the percentage of pacemaker-like

cells, suggesting that the role of endothelin-1 in CCS development may be conserved, even in mice (Gassanov et al., 2004).

Mesp1 and *Mesp2* are transcription factors that contain almost identical basic helix–loop–helix (bHLH) motifs and are encoded by genes that both localize in chromosome 7 (Saga et al., 1996, 1997). Disruption of the *Mesp1* gene results in cardia bifida (Saga, 1998). We also have shown previously, using double knockout mouse embryos and by chimera analysis, that *Mesp1* and *Mesp2* are essential for the development of cardiac mesoderm (Kitajima et al., 2000). *Mesp1* expression is restricted to the nascent mesodermal cells, and its expression is transient and down-regulated before heart tube formation (Saga et al., 1999). However, lineage analysis using *Mesp1-cre* has revealed that *Mesp1*-expressing cells are incorporated into almost all of the precursors of the cardiovascular system (i.e., endothelium, endocardium, myocardium, and epicardium), both in embryonic and extraembryonic regions at 9.5 dpc, and that *Mesp1* expression is the earliest detectable molecular marker in heart precursor cells (Saga et al., 1999, 2000). In this current study, we describe further detailed lineage analyses of the mouse heart using *Mesp1-cre* mice. We show that *Mesp1*-nonexpressing cells contribute to neural crest-derived regions as well as to a subset of the cells in the ventricular CCS.

RESULTS

Lineage Analysis of *Mesp1*-Expressing Mesodermal Cells in the Developing Heart

Using *Mesp1-cre*-mediated cell lineage analysis, we previously reported that *Mesp1*-expressing cells were incorporated into almost all precursors of the cardiovascular system in both embryonic and extraembryonic regions at 9.5 dpc (Saga et al., 2000). However, further analysis at 13.5 dpc now has revealed that the cardiogenic cells are not entirely contributed by *Mesp1*-expressing cells, suggesting that the origin of these cells may be subdivided according to *Mesp1* expression (Fig. 1A–C). At this developmen-

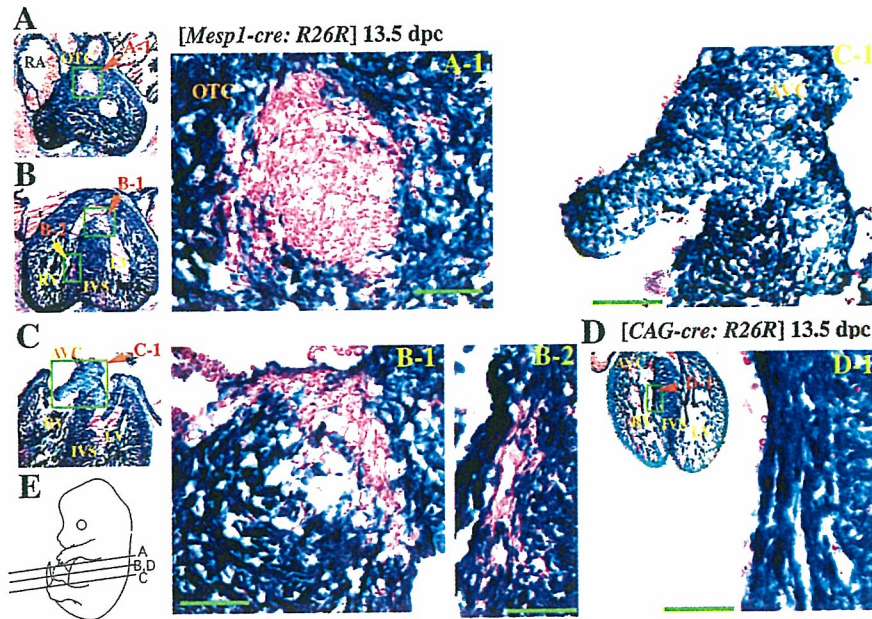


Fig. 1. Transverse sections of β -galactosidase (β -gal) -stained *Mesp1-cre:R26R* or *CAG-cre:R26R* embryos at 13.5 days post coitum (dpc). **A–B:** The β -gal-negative areas were observed in the region of outflow tract cushions (OTC; A; boxed area in A-1) and along the interventricular septum (IVS) in a pattern reminiscent of the ventricular cardiac conduction system (CCS; B; boxed areas, B-1 and B-2). **C:** atrioventricular cushions (AVC; boxed area in C-1) showed β -gal activity. Original magnification, $\times 100$. Magnified images of OT cushion cells, the interventricular regions, and AV cushions are shown in A-1, B-1 and -2, and C-1, respectively. **D:** Transverse sections of β -gal-stained *CAG-cre:R26R* embryos show no β -gal-negative regions, suggesting that *R26R* expression was not shut down as *Mesp1*-nonexpressing cells differentiate. A magnified image in the interventricular regions is shown in D-1. **E:** Sectioning planes are illustrated and were counterstained with eosin. LV, left ventricle; RA, right atrium; RV, right ventricle. Scale bar = 100 μ m.

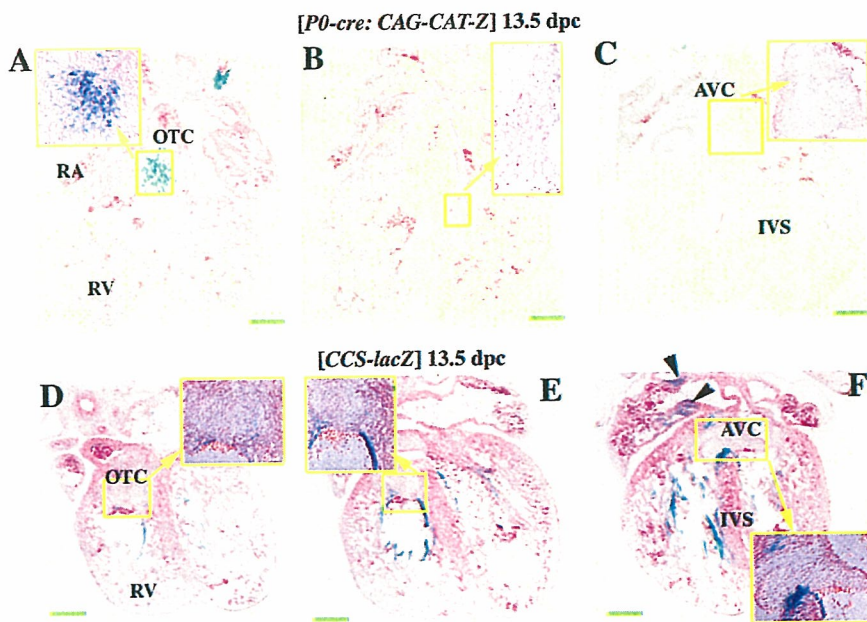


Fig. 2. β -galactosidase (β -gal) staining in sections of the *P0-cre:CAG-CAT-Z* and the *CCS-lacZ* embryos at 13.5 days post coitum (dpc). **A–C:** In the *P0-cre:CAG-CAT-Z* embryo, high β -gal activity is observed in the region of the outflow tract cushion (OTC; A, boxed area), but little activity is evident in the region of the atrioventricular cushion (AVC; C, boxed area). Original magnification, $\times 40$. Note that the β -gal activity was not observed within the ventricle and the interventricular septum (IVS; B). **D–F:** The images in the boxed area are magnified. In the *CCS-lacZ* embryo, β -gal activity is observed strongly in part of the atria (indicated by arrowheads) and along the IVS in a pattern reminiscent of the ventricular cardiac conduction system (CCS; boxed area). In contrast, β -gal activity in either the OTC or AVC regions was barely detectable (D,F). The images in the boxed area are magnified. Sectioning planes of images A–C and D–F are the same as those illustrated in Figure 1E: A–C, respectively. All sections were counterstained with eosin. RA, right atrium; RV, right ventricle. Scale bar = 200 μ m.

tal stage (13.5 dpc), during which the septation complexes start to form, *Mesp1*-nonexpressing cells are also visible along the IVS region in a pattern reminiscent of the AVB and bundle branches, which are components of the ventricular CCS (Fig. 1B). In addition, region of the OT cushions had little β -gal activity (Fig. 1A), unlike most of the AV cushions that had strong activity (Fig. 1C). In the *CAG-cre* mouse, in which the *cre* gene is under the control of the cytomegalovirus immediate early enhancer-chicken beta-actin hybrid (*CAG*) enhancer, it has been reported that the sequence between the two *loxP* sites is deleted in all tissues in the mouse embryo (Sakai and Miyazaki, 1997). This finding was confirmed in our current experiments; all of the cells in the developing heart of double-transgenic embryos were positive for *LacZ* (Fig. 1D), indicating that this expression is not down-regulated upon *CAG* promoter activation. This observation strongly suggests that *Mesp1*-“non” expressing cells are indeed present in the developing murine heart of the *Mesp1-cre:R26R* reporter double-transgenic mouse.

Because neural crest cells are known to contribute to part of the developing heart structure (Jiang et al., 2000), we initially expected that the regions containing *Mesp1*-nonexpressing cells might reflect this population. To address this possibility more fully, we next compared our findings with a previous report that used a *P0-cre* transgene and *CAG-CAT-Z* reporter gene to identify neural crest-derived cells (Yamauchi et al., 1999).

Mesp1-Nonexpressing Cells Along the Ventricular Septum Are Not Derived From the Neural Crest

We analyzed *P0-cre:CAG-CAT-Z* embryos to examine whether neural crest cells indeed contribute to any of the regions occupied by *Mesp1*-nonexpressing cells. In the *P0-cre:CAG-CAT-Z* embryo at 13.5 dpc, β -gal activity was mainly detected in the mesenchyme located within the OT cushions of the heart (Fig. 2A), which is consistent with previous findings (Yamauchi et al., 1999) and a report using *Wnt1-cre* mice (Jiang et al.,

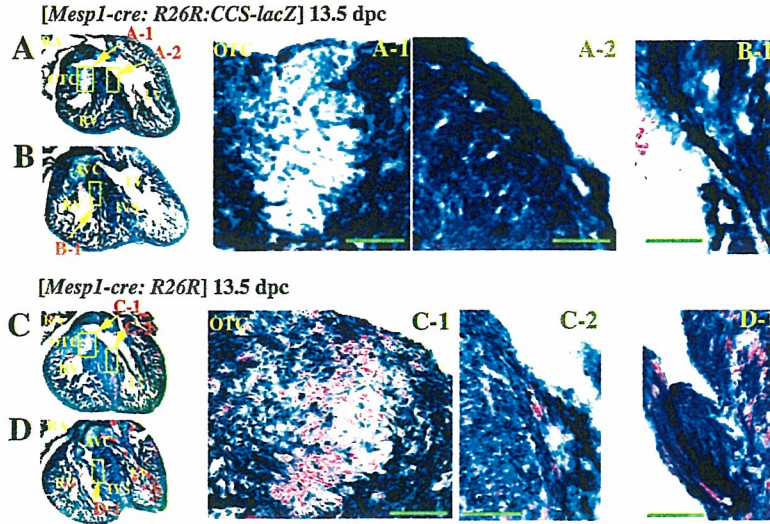


Fig. 3.

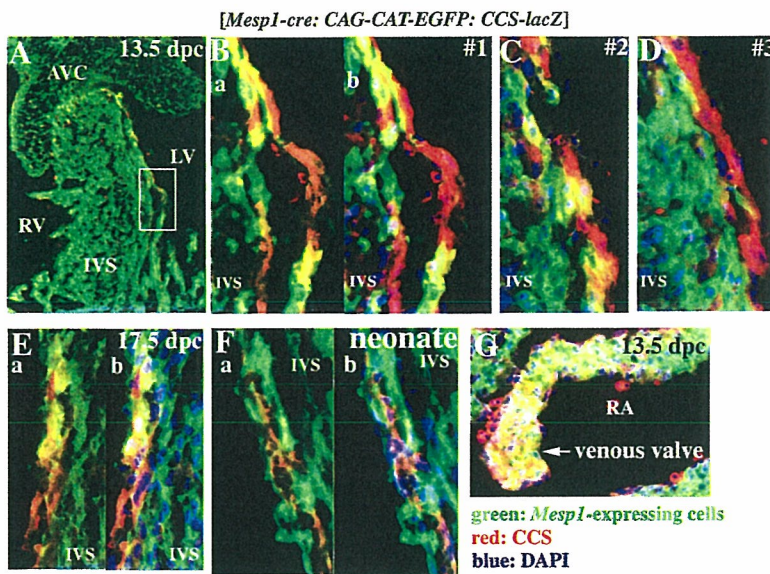


Fig. 4.

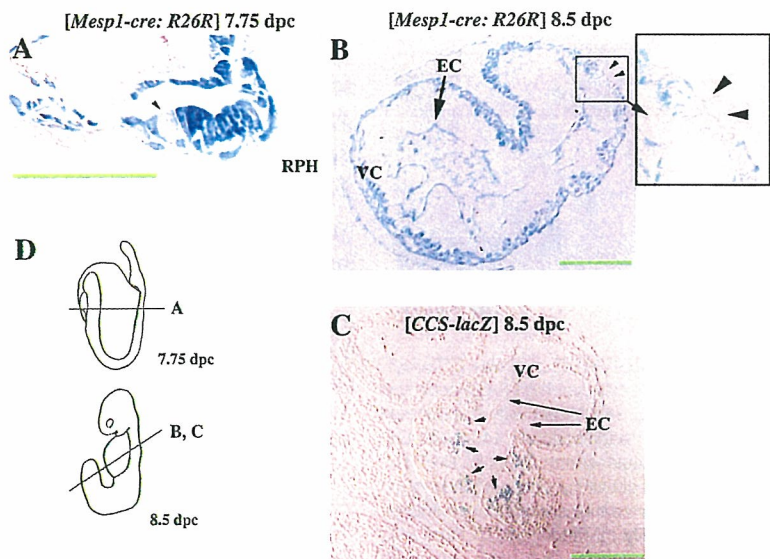


Fig. 5.

Fig. 3. Comparison of β -gal staining patterns between *Mesp1-cre:R26R:CCS-lacZ* triple hetero-embryos and *Mesp1-cre:R26R* embryos. **A,B:** Sections of the heart of the *Mesp1-cre:R26R:CCS-lacZ* embryo at 13.5 days post coitum (dpc). **C,D:** Compared with the *Mesp1-cre:R26R* embryo (boxes in C-2 and D-1), *Mesp1*-nonexpressing cells along the interventricular (IVS) were barely observed in the *Mesp1-cre:R26R:CCS-lacZ* triple hetero-embryos (A,B; boxes in A-2 and B-1). However, *Mesp1*-nonexpressing cells in outflow tract (OT) cushion regions were also detected, even in the triple hetero-embryos (box A-1). Original magnification, $\times 100$. The images in the boxed area are magnified. Sectioning planes of A, B, and C, D are the same as those illustrated in Figure 1E: B and C, respectively. Sections were counterstained with eosin; AVC, atrioventricular cushion; IVS, interventricular septum; RA, right atrium; RV, right ventricle; Scale bar = 100 μ m.

Fig. 4. *Mesp1*-nonexpressing cells contribute to a subset of the ventricular cardiac conduction system (CCS). Triple immunostaining for *Mesp1*-expressing cells (green fluorescent protein [GFP]-positive cells; green), cells of the ventricular CCS (LacZ-positive cells; red), and nuclei (4',6'-diamidino-2-phenylindole [DAPI] staining; blue) in a *Mesp1-cre:CAG-CAT-EGFP:CCS-lacZ* embryo. All images shown are merged views, and double immunostaining of GFP and LacZ (a) and a triple immunostaining image with additional DAPI staining (b) are shown in some cases. **A-D:** A merged view of the interventricular (IVS) region at 13.5 days post coitum (dpc). The boxed area of the ventricular CCS in A was magnified as shown in B. Other sections derived from additional embryos are shown in C and D. The presence of red cells suggests that *Mesp1*-nonexpressing cells actually belong to the ventricular CCS, whereas some *Mesp1*-expressing cells also colocalize here (yellow). Typical images of mixed cell populations are shown in B and C, whereas a red cell-dominant section is shown in D. Original magnification, $\times 400$, except for A, which is $\times 100$. **E,F:** Merged view in the IVS region in an embryo at 17.5 dpc (E) or in a neonate (F). Original magnification, $\times 400$. Red cells (i.e., the *Mesp1*-nonexpressing cells belonging to the CCS) were observed even at later stages beyond 13.5 dpc. **G:** The region of the venous valves, which are proposed remnants of the embryonic sinoatrial (SA) ring, at 13.5 dpc. Almost all of the cells in this region were stained yellow, suggesting that the cells belonging to the venous valves are *Mesp1*-expressing. Original magnification, $\times 200$. Sectioning planes are those between B and C, illustrated in Figure 1E. AVC, atrioventricular cushion; LV, left ventricle; OT, outflow tract cushion; RA, right atrium; RV, right ventricle.

Fig. 5. Comparison of transverse sections of β -gal stained *Mesp1-cre:R26R* embryos with *CCS-lacZ* embryos at an earlier stage. **A:** At 7.75 days post coitum (dpc) in *Mesp1-cre:R26R* embryos, we observed a few *Mesp1*-nonexpressing cells within the primitive heart tube (arrow head). Original magnification, $\times 400$. **B:** At 8.5 dpc, the regions of the *Mesp1*-nonexpressing cells in *Mesp1-cre:R26R* embryos, were observed more clearly (arrowheads). **C:** The β -gal-positive regions (i.e., the cells belonging to the CCS) were observed mainly in the sub-endocardial myocardium of 8.5 dpc *CCS-lacZ* mouse (arrows). Original magnification, $\times 200$. **D:** Sectioning planes are illustrated. Sections were counterstained with eosin. EC, endocardium; RPH, right primitive heart tube; VC, ventricular chamber. Scale bars = 100 μ m.

2000). There were only minimal contributions by neural crest cells in the AV cushions, as predicted by the β -gal activity in the *Mesp1-cre:R26R* mouse (Fig. 2C). Importantly, however, neural crest-derived mesenchyme was not observed in either part of the ventricle or the IVS (Fig. 2B), where *Mesp1*-nonexpressing cells were visible (Fig. 1B). This finding indicates that other cell types must contribute to this particular region. Intriguingly, the distribution of *Mesp1*-nonexpressing cells resembled that of the AVB and bundle branches and also the Purkinje fibers of the CCS. This prompted us to speculate that ventricular CCS cells might be derived from lineages that are distinct from both the neural crest and *Mesp1*-expressing mesodermal cells.

Mesp1-Nonexpressing Cells Contribute to the CCS

As a preliminary approach to determine whether or not *Mesp1*-nonexpressing cells did in fact reside in the CCS, we compared these cells with the β -gal expression patterns in embryonic hearts of *CCS-lacZ* transgenic mice. In these mice, the specialized CCS can be visualized by β -gal activity (Rentschler et al., 2001). In 13.5 dpc hearts from these transgenic animals, strong β -gal activity could be observed in part of the atrium, which could correspond to the SA node. This high level of activity could also be detected along the IVS, which demarcates the ventricular CCS, including the AVB and bundle branches (Fig. 2D–F). When comparing these results with those shown in Figure 1, the portion of the *Mesp1*-nonexpressing cell population along the IVS was found to show a similar pattern to the β -gal-positive regions in the *CCS-lacZ* mice, suggesting that these *Mesp1*-nonexpressing cells contribute to the ventricular CCS.

To provide direct evidence for our hypothesis that cells of the ventricular CCS are indeed derived from *Mesp1*-nonexpressing cells, we generated triple transgenic *Mesp1-cre:R26R:CCS-lacZ* mice. Because both the *CCS-lacZ* and *R26R* transgenic mice use β -gal as a marker, the entire region contributed by the *Mesp1*-nonexpressing cells in the IVS would become β -gal-positive in the triple hetero-embryonic

hearts if our contention was correct. As shown in Figure 3, this was found to be the case, as all of the cells in the IVS had β -gal activity, which was in contrast to the corresponding sections of the *Mesp1-cre:R26R* embryo (Fig. 3C,D). Moreover, the region of the OT cushions had little β -gal activity even in the triple hetero-embryo (Fig. 3A), supporting our conclusion that this region is occupied mainly by cells of neural crest origin. Hence, these data suggest that the *Mesp1*-nonexpressing cells in the IVS belong to the ventricular CCS.

It was still unclear, however, whether all of the ventricular CCS is derived from *Mesp1*-nonexpressing cells, because both the *CCS-lacZ* and *R26R* reporter mice use the same β -gal marker. We, therefore, performed a similar series of studies using the *CAG-CAT-EGFP* strain (Kawamoto et al., 2000), in which GFP expression is dependent upon cre-mediated recombination and representative results are shown in Figure 4. *Mesp1*-nonexpressing cells at 13.5 dpc do indeed reside within the ventricular CCS (*Mesp1*-nonexpressing/*CCS-lacZ*-positive red cells in Fig. 4A–D), although it is clear that the CCS is also observed in the *Mesp1*-expressing cell populations (i.e., *Mesp1*-expressing/*CCS-lacZ*-positive yellow cells). In addition, after 4',6'-diamidino-2-phenylindole (DAPI) staining, we observed that all of the green fluorescent protein (GFP)-negative *Mesp1*-nonexpressing cells belonged to the *lacZ*-positive cells of the ventricular CCS, because cells positive for DAPI alone (blue) were rarely observed along the IVS (b in Fig. 4A–C). To demonstrate the heterocellular origin of CCS more unequivocally and to analyze the ratios quantitatively, we generated serial sections of the embryonic heart along the anteroposterior axis and analyzed the staining patterns.

A total of three embryos were sectioned and 58 sections containing CCS-LacZ staining in the IVS region were further subjected to semiquantitative analysis (Supplementary Figure S1, which can be viewed at <http://www.interscience.wiley.com/jpages/1058-8388/suppmat>). However, as the CCS distributes peripherally in the IVS with multiple branchings, it is very difficult to quantify. We, there-

fore, roughly estimated the ratio by counting DAPI stained nuclei in each cell type and selected 28 typical sections, from which 16 showed a colocalization pattern for yellow and red cells (Fig. 4B,C). Of these 16 sections, 2 and 5 showed a red cell- and a yellow cell-dominant pattern, respectively (Fig. 4D, and data not shown). We have estimated that approximately 20% of the ventricular CCS, along the IVS, corresponds to *Mesp1*-nonexpressing cells. Moreover, red cells (i.e., the *Mesp1*-nonexpressing cells belonging to the ventricular CCS) were also observed in the ventricular CCS even at later developmental stages of 17.5 dpc (Fig. 4E) and in neonates at 4 days after birth (Fig. 4F). The AV cushion cells were weakly positive for the GFP signal, due to the thinness of the cytoplasm and resulting lower intensity of fluorescence (Fig. 4A), but their identity was confirmed by LacZ staining in *Mesp1-cre; R26R* embryos (Fig. 1C). Thus, we conclude unequivocally that the population of *Mesp1*-nonexpressing cells, which we identified along the ventricular septum, contributes to the CCS.

In the case of the SA or AV node regions of the CCS, the contribution of *Mesp1*-expressing and/or *Mesp1*-nonexpressing cells was not as clear from our present results using embryos at 13.5 dpc, because these typical node structures were not discernible. In contrast, we were able to determine that most of the cells in the venous valves, which are the proposed remnants of the embryonic SA ring in the fully developed heart (Rentschler et al., 2001), of the *Mesp1-cre:CAG-CAT-EGFP:CCS-lacZ* embryo were *Mesp1*-expressing (i.e., GFP-positive cells). This determination was revealed by the *Mesp1*-expressing/*CCS-lacZ*-positive yellow cells at 13.5 dpc (Fig. 4G). However, the developmental relationships between the venous valves and both the SA and AV nodes have not yet been determined.

Origin of *Mesp1*-Nonexpressing Cells

To determine the origin of the *Mesp1*-nonexpressing cells, we examined the *LacZ* expression profiles in more immature *Mesp1-cre:R26R* and *CCS-lacZ* embryos. As shown in Figure 5A,

even at 7.75 dpc, at which stage the cardiac crescent can be observed, a few β -gal-negative cells were detectable in the *Mesp1-cre:R26R* embryo. The β -gal-negative cells were observed in the myocardium region more clearly at 8.5 dpc (Fig. 5B). In the *CCS-lacZ* embryo, although the heart region at 7.75 dpc was confirmed to be β -gal-negative (data not shown) as reported previously (Rentschler et al., 2001), patchy staining was observed mainly in the subendocardial myocardium region at 8.5 dpc (Fig. 5C). However, a direct relationship between the *Mesp1*-nonexpressing cells and the CCS cells is still not clear, although the neural crest cells, which are also identifiable as *Mesp1*-nonexpressing cells in our system, have not yet arrived in the heart at this stage and can be excluded (Jiang et al., 2000).

DISCUSSION

In this study, we have found using a *Cre-loxP* site-specific recombination system that the origin of the cardiac mesenchyme is subdivided according to the presence of *Mesp1* expression. We demonstrate that the regions occupied by *Mesp1*-nonexpressing cells correspond to two distinct populations of cells: one derived from the neural crest and the other one that contributes to the ventricular CCS.

Comparison of the Cell-Lineages of Neural Crest Cells and *Mesp1*-Nonexpressing cells

In our experiments with *Mesp1-cre:R26R* embryos, we have found that cells derived from the neural crest are negative but that mesodermal cells derived from *Mesp1*-expressing cells are positive, for β -gal activity. We have also confirmed that mammalian cardiac neural-crest cells are *Mesp1*-negative (Figs. 1, 2) and contribute to the mesenchyme in the OT cushions of the heart. These observations were made following neural crest cell lineage analyses using the *P0-cre:CAG-CAT-Z* strain (Fig. 2) and are consistent with previous results obtained using *Wnt1-cre:R26R* double transgenic mice (Jiang et al., 2000). The origin of the cells of the AV cushions was suggested to be mesodermal, because this region was occupied by *Mesp1*-expressing cells in our study

(Fig. 1C). This result is consistent with the previous study of Kisanuki et al. (2001) using *Tie2-cre* mice that reported that the origin of the AV cushions is mainly of endocardial cell lineage. Thus, mesenchymal cells in the OT cushions are derived from mainly neural crest cells and those in the AV cushions are derived from endocardium.

Importantly, we observed a second population of *Mesp1*-nonexpressing cells, along the IVS (Fig. 1B). Because this region is not contributed by neural crest cells (Fig. 2B), we explored the possibility that these *Mesp1*-nonexpressing cells reside in the ventricular CCS. Before examining this possibility, we first confirmed that the failure to express β -gal in the *Mesp1-cre:R26R* embryos was not due to an artifact, such as down-regulation of *LacZ* expression during differentiation or mosaicism of Cre recombinase expression. To exclude the former possibility, we examined *CAG-cre:R26R* mice, in which Cre recombinase is ubiquitously expressed and all cells should be *LacZ*-positive. We did not subsequently observe any *LacZ*-negative cells in the heart, indicating that there had been no down-regulation of *LacZ* upon cell differentiation (Fig. 1D). To exclude possible mosaicism of Cre recombinase, we repeated our analysis in more than 20 embryos and observed very consistent results, although some clonal differences may exist. In addition, when we crossed the *Mesp1-cre* and *CCS-lacZ* strains and monitored *R26R*-dependent reporter gene expression, we did not observe patchy *LacZ*-negative cells in the ventricular wall. Thus, it appears unlikely that mosaicism of the *R26R* reporter could account for our results.

As for the contribution of the neural crest cells into the ventricular CCS, it was reported that neural crest-derived cells were observed in the vicinity of the CCS in the IVS at 14.5 dpc using the *Wnt1-cre:R26R* reporter system (Poelmann et al., 2004). Thus, the possibility cannot be ruled out that the neural crest cells contribute to CCS in the IVS, although we could not detect any β -gal-positive cells in the IVS in our *P0-cre:CAG-CAT-Z* system. The discrepancy could be due to the difference in systems used for lineage analyses. The future studies using triple transgenic strategy (*Wnt1-cre:CAG-*

CAT-GFP:CCS-lacZ) as used in our current study would be useful to discriminate the discrepancy.

Origins of the CCS

Using *Mesp1-cre:R26R* embryos, we identified a population of *Mesp1*-nonexpressing cells that were found to be distributed in the wall along the ventricular septum (Fig. 1B). The results of genetic crosses with the *CCS-lacZ* strain suggested that these *Mesp1*-nonexpressing cells contribute to the ventricular CCS (Fig. 3B). To confirm these findings, we generated triple transgenic *Mesp1-cre:CAG-CAT-EGFP:CCS-lacZ* mice. Double-staining for GFP and β -gal expression and/or additional DAPI staining in these mice confirmed that the *Mesp1*-nonexpressing cells contribute approximately 20% of the ventricular CCS (Fig. 4). Moreover, these populations of cells can be distinguished at a stage as early as stage 7.75 dpc at least (Fig. 5), whereas *Mesp1* is initially, albeit transiently, expressed at 6.5 dpc (Saga et al., 1996).

The pacemaking and conduction systems of the heart are composed of the SA node, AV node, AVB, the bundle branches, and the Purkinje fibers, each of which can be distinguished morphologically, functionally, and molecularly (Moorman and Christoffels, 2003). The origin of the nodal tissue is less clear than that of the ventricular CCS, although the primary myocardium is suggested to be a candidate (Moorman and Christoffels, 2003). Recently, it was suggested that some of the working myocardium could also differentiate into nodal tissues, even after birth (Pashmforoush et al., 2004). Although the developmental relationships between the venous valves and the nodes have not yet been fully elucidated, our data indicate that most of cells in the venous valves, which are proposed to be remnants of the embryonic SA ring (Rentschler et al., 2001), are derived from *Mesp1*-expressing cells (Fig. 4G). However, further detailed studies will be required to determine the precise cellular origin of the nodes and their relationships with the venous valves.

In the present analyses, we have focused on the cell-lineages of the ventricular CCS and shown them to be of

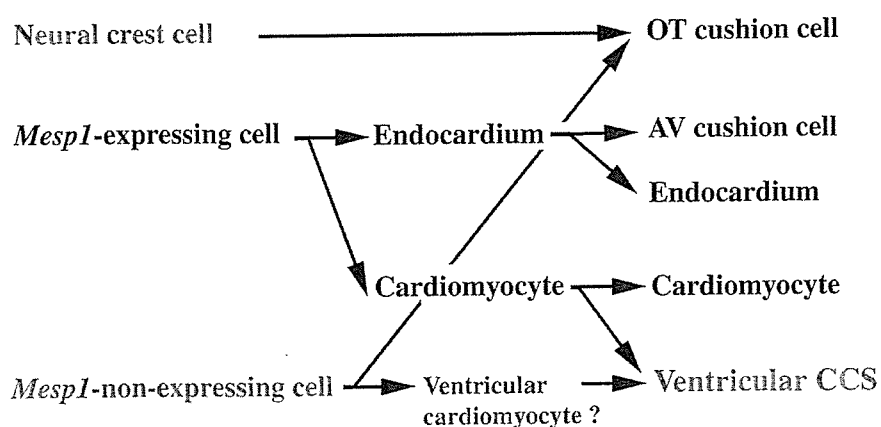


Fig. 6. Summary of the origin and cell-fate relationships of cardiac mesenchyme cell types. Each cardiac cell type is established by three distinct origins: neural crest cells, the mesodermal cells of *Mesp1*-expressing cells, and *Mesp1*-nonexpressing cells. It is noteworthy that both the *Mesp1*-expressing cells and the *Mesp1*-nonexpressing cells contribute to the ventricular CCS. In addition, the origins of the subset of the ventricular CCS that are contributed by the *Mesp1*-nonexpressing cells are distinguishable from that of the myocardium by the *Mesp1* expression profile. We speculate that the *Mesp1*-nonexpressing cardiomyocyte may be a candidate for the origin of the subset of the ventricular CCS. [Color figure can be viewed in the online issue, which is available at www.interscience.wiley.com.]

heterocellular origin. Two possibilities have emerged from both our analyses and previous reports concerning the origin of the ventricular CCS in mouse, occupied by *Mesp1*-nonexpressing cells. First, it is conceivable that the *Mesp1*-nonexpressing cells in the CCS are not derived from cardiomyocytes. Alternatively, these cells may represent cardiomyocytes, which simply do not express *Mesp1*. We favor this latter possibility. Lineage tracing experiments in chick have convincingly demonstrated that the ventricular CCS, including the Purkinje fibers, are derived from cardiomyocytes (reviewed in Mikawa, 1999; Pennisi et al., 2002). Moreover, experiments in the mouse also indicate that embryonic cardiomyocytes can be converted to a CCS-like phenotype in response to neuregulin-1, at least when assayed by up-regulation of the *CCS-lacZ* transgene (Rentschler et al., 2002). Nonetheless, additional analyses will be required to determine the basis for the molecular heterogeneity within the ventricular CCS and to determine whether there is associated functional diversity in this structure.

In conclusion, we have determined that *Mesp1*-nonexpressing cells contribute to the ventricular CCS in addition to the OT cushion. Furthermore, we indicate a possibility that a population of the cells that contribute to the ventricular CCS might be distinguished at an early stage of de-

velopment. Unfortunately, it could not be clarified from our present experiments whether *Mesp1*-nonexpressing cells also contributed to the other regions of the CCS, such as the SA or AV nodes. A scheme summarizing the cell lineage relationships in the developing murine heart is shown in Figure 6. Our observation that the ventricular CCS includes both *Mesp1*-expressing and -nonexpressing cells is evidence of the heterogeneous nature of the ventricular CCS. The further identification of specific molecular markers for the mouse CCS, expressed at early embryonic stages, will undoubtedly enhance our understanding of the developmental biology of the CCS in the heart.

EXPERIMENTAL PROCEDURES

Lineage Analysis of *Mesp1*-Expressing Cells

The *Mesp1-cre* knockin mouse was constructed by introduction of a gene encoding Cre recombinase into the *Mesp1* locus, as previously described (Saga et al., 1999). The fidelity of expression was confirmed by in situ hybridization at E7.0 (data not shown). Genotyping was performed by polymerase chain reaction using a neo-specific primer NeoAL2: 5'-GGGGATGCGGTGGGCTCTATGGCTT-3' and *Mesp1* primer MesP1-GR1: 5'-ATATGCCAAGTCATTGAGGTGAGCTTTC-3'. *Mesp1-cre* mice

were crossed with either *CAG-CAT-Z* (Araki et al., 1995), *R26R* (Soriano, 1999), or *CAG-CAT-EGFP* (Kawamoto et al., 2000) reporter mice. *P0-cre* (Yamauchi et al., 1999) and *CCS-lacZ* mice (Rentschler et al., 2001) were also used for cell lineage analyses. Mice were maintained on a 7:00 AM to 7:00 PM light-dark cycle, with noon on the day of vaginal plug discovery defined as 0.5 dpc.

β -gal Staining, Immunostaining, and In Situ Hybridization

Embryos that had been fixed at 7.5–10.5 dpc were stained for the detection of β -galactosidase activity in whole-mounts as described previously (Saga et al., 1992). The specimens were then dehydrated by means of a graded ethanol series, embedded in either paraffin wax or plastic resin (technovit 8100, Heraeus Kulzer, Inc.) and sectioned at a thickness of 4 μ m. Hearts that had been isolated from embryos at later stages were subjected to β -gal staining after sectioning. Briefly, hearts were fixed in a solution of 2% paraformaldehyde, 0.05% glutaraldehyde, and 0.02% NP-40 in phosphate buffer (PBS) for 30 min on ice. The tissues were then sequentially soaked in a graded series of 10, 20, and 30% sucrose (w/v) in PBS while being gently agitated on a shaking platform, culminating in a 50:50 mix of 30% sucrose:OCT. Samples were frozen and stored at -80°C until sectioning at 8 μ m thickness, and the sections were placed on gelatin-coated slides. Frozen sections of *Mesp1-cre:CAG-CAT-EGFP:CCS-lacZ* mouse hearts was stained with anti-lacZ and anti-GFP antibodies as follows: sections prepared were fixed with 4% paraformaldehyde for 3 min, treated with 10 μ g/ml proteinase K and blocked in 3% skim milk for 30 min at room temperature (RT). Blocking solutions was replaced with rabbit anti- β -gal antibody (Cappel, ICN Pharmaceuticals, Inc., OH) at a dilution of 1:2,000 and with rat anti-GFP antibody (Nacalai Tesque, Kyoto, Japan) at a dilution 1:200 and incubated overnight at 4°C . After brief washes in PBS, the sections were incubated with Alexa 594-conjugated anti-rabbit followed by Alexa 488-conjugated anti-rat secondary antibodies at dilutions of 1:200

for 90 min at RT. These sections were then incubated with 0.1 µg/ml of DAPI (Sigma, St. Louis, MO) for 5 min to visualize nuclei.

ACKNOWLEDGMENTS

We thank the following researchers for providing mice: Dr. Jun-ichi Miyazaki (*CAG-cre*, *CAG-CAT-Z*, and *CAG-CAT-EGFP*), Dr. Kuniya Abe (*P0-cre*), Dr. Philippe Soriano (*R26R*), and Dr. Glenn I. Fishman (*CCS-lacZ*). We also thank Seiko Shinzawa, Mariko Ikumi, Eriko Ikeno, Chizuko Obata, Shinobu Watanabe, and Maho Endo for technical assistance.

REFERENCES

- Araki K, Araki M, Miyazaki J, Vassalli P. 1995. Site specific recombination of a transgene in fertilized eggs by transient expression of Cre recombinase. *Proc Natl Acad Sci U S A* 92:160–164.
- Cheng G, Litchenberg WH, Cole GJ, Mikawa T, Thompson RP, Gourdie RG. 1999. Development of the cardiac conduction system involves recruitment within a multipotent cardiomyogenic lineage. *Development* 126:5041–5049.
- Coppen SR, Dupont E, Rothery S, Severs NJ. 1998. Connexin45 expression is preferentially associated with the ventricular conduction system in mouse and rat heart. *Circ Res* 82:232–243.
- Coppen SR, Severs NJ, Gourdie RG. 1999. Connexin45 (alpha 6) expression delineates an extended conduction system in the embryonic and mature rodent heart. *Dev Genet* 24:82–90.
- Delorme B, Dahl E, Jarry-Guichard T, Marics I, Briand JP, Willecke K, Gros D, Theveniau-Ruissy M. 1995. Developmental regulation of connexin 40 gene expression in mouse heart correlates with the differentiation of the conduction system. *Dev Dyn* 204:358–371.
- Gassanov N, Er F, Zagidullin N, Hoppe UC. 2004. Endothelin induces differentiation of ANP-EGFP expressing embryonic stem cells towards a pacemaker phenotype. *FASEB J* 18:1710–1712.
- Gourdie RG, Mima T, Thompson RP, Mikawa T. 1995. Terminal diversification of the myocyte lineage generates Purkinje fibers of the cardiac conduction system. *Development* 121:1423–1431.
- Jiang X, Rowitch DH, Soriano P, McMahon AP, Sucov HM. 2000. Fate of the mammalian cardiac neural crest. *Development* 127:1607–1616.
- Kawamoto S, Niwa H, Tashiro F, Sano S, Kondoh G, Takeda J, Tabayashi K, Miyazaki J. 2000. A novel reporter mouse strain that expresses enhanced green fluorescent protein upon Cre-mediated recombination. *FEBS Lett* 470:263–268.
- Kirby ML, Gale TF, Stewart DE. 1983. Neural crest cells contribute to normal aorticopulmonary septation. *Science* 220:1059–1061.
- Kisanuki YY, Hammer RE, Miyazaki J, Williams SC, Richardson JA, Yanagisawa M. 2001. Tie2-Cre transgenic mice: a new model for endothelial cell-lineage analysis in vivo. *Dev Biol* 230:230–242.
- Kitajima S, Takagi A, Inoue T, Saga Y. 2000. *MesP1* and *MesP2* are essential for the development of cardiac mesoderm. *Development* 127:3215–3226.
- Kupersmidt S, Yang T, Anderson ME, Wessels A, Niswender KD, Magnuson MA, Roden DM. 1999. Replacement by homologous recombination of the minK gene with lacZ reveals restriction of minK expression to the mouse cardiac conduction system. *Circ Res* 84:146–152.
- Mikawa T. 1999. Cardiac lineages. In: Harvey RP, Rosenthal N, editors. *Heart development*. San Diego: Academic Press. p 19–33.
- Moorman AFM, Christoffels VM. 2003. Cardiac chamber formation: development, genes, and evolution. *Physiol Rev* 83:1223–1267.
- Moorman AFM, deJong F, Denyn MM, Lamers WH. 1998. Development of the cardiac conduction system. *Circ Res* 82:629–644.
- Myers DC, Fishman GI. 2004. Toward an understanding of the genetics of murine cardiac pacemaking and conduction system development. *Anat Rec A Discov Mol Cell Evol Biol* 280:1018–1021.
- Nguyen-Tran VT, Kubalak SW, Minamisawa S, Fiset C, Wollert KC, Brown AB, Ruiz-Lozano P, Barrere-Lemaire S, Kondo R, Norman LW, et al. 2000. A novel genetic pathway for sudden cardiac death via defects in the transition between ventricular and conduction system cell lineages. *Cell* 102:671–682.
- Pashmforoush M, Lu JT, Chen H, Amand TS, Kondo R, Pradervand S, Evans SM, Clark B, Feramisco JR, Giles W, Ho SY, Benson DW, Silberbach M, Shou W, Chien KR. 2004. *Nkx2-5* pathways and congenital heart disease; loss of ventricular myocyte lineage specification leads to progressive cardiomyopathy and complete heart block. *Cell* 117:373–386.
- Pennisi DJ, Rentschler S, Gourdie RG, Fishman GI, Mikawa T. 2002. Induction and patterning of the cardiac conduction system. *Int J Dev Biol* 46:765–775.
- Poelmann RE, Jongbloed MR, Molin DG, Fekkes ML, Wang Z, Fishman GI, Doetschman T, Azhar M, Gittenberger-de Groot AC. 2004. The neural crest is contiguous with the cardiac conduction system in the mouse embryo: a role in induction? *Anat Embryol (Berl)* 208:389–393.
- Rentschler S, Vaidya DM, Tamaddon H, Degenhardt K, Sassoon D, Morley GE, Jalife J, Fishman GI. 2001. Visualization and functional characterization of the developing murine cardiac conduction system. *Development* 128:1785–1792.
- Rentschler S, Zander J, Meyers K, France D, Levine R, Porter G, Rivkees SA, Morley GE, Fishman GI. 2002. Neuregulin-1 promotes formation of the murine cardiac conduction system. *Proc Natl Acad Sci U S A* 99:10464–10469.
- Saga Y. 1998. Genetic rescue of segmentation defect in *MesP2*-deficient mice by *MesP1* gene replacement. *Mech Dev* 75:53–66.
- Saga Y, Yagi T, Ikawa Y, Sakakura T, Aizawa S. 1992. Mice develop normally without tenascin. *Genes Dev* 6:1821–1831.
- Saga Y, Hata N, Kobayashi S, Magnuson T, Seldin M, Taketo MM. 1996. *MesP1*: a novel basic helix-loop-helix protein expressed in the nascent mesodermal cells during mouse gastrulation. *Development* 122:2769–2778.
- Saga Y, Hata N, Koseki H, Taketo MM. 1997. *Mesp2*: a novel mouse gene expressed in the presegmented mesoderm and essential for segmentation initiation. *Genes Dev* 11:1827–1839.
- Saga Y, Miyagawa-Tomita S, Takagi A, Kitajima S, Miyazaki J, Inoue T. 1999. *MesP1* is expressed in the heart precursor cells and required for the formation of a single heart tube. *Development* 126:3437–3447.
- Saga Y, Kitajima S, Miyagawa-Tomita S. 2000. *Mesp1* expression is the earliest sign of cardiovascular development. *Trends Cardiovasc Med* 10:345–352.
- Sakai K, Miyazaki J. 1997. A transgenic mouse line that retains Cre recombinase activity in mature oocytes irrespective of the cre transgene transmission. *Biochem Biophys Res Commun* 237:318–324.
- Soriano P. 1999. Generalized lacZ expression with the ROSA26 Cre reporter strain. *Nat Genet* 21:70–71.
- Waldo K, Miyagawa-Tomita S, Kumiski D, Kirby ML. 1998. Cardiac neural crest cells provide new insight into septation of the cardiac outflow tract: aortic sac to ventricular septal closure. *Dev Biol* 196:129–144.
- Yamauchi Y, Abe K, Mantani A, Hitoshi Y, Suzuki M, Osuzu F, Kuratani S, Yamamura K. 1999. A novel transgenic technique that allows specific marking of the neural crest cell lineage in mice. *Dev Biol* 212:191–203.